1-24-96

SANDIA REPORT

SAND95–2352 • UC–704
Unlimited Release
Printed December 1995

Characterization of E-Glass/Polyester Woven Fabric Composite Laminates and Tubes

T. R. Guess, E. D. Reedy, Jr., M. E. Stavig

Prepared by
Sandia National Laboratories
Albuquerque, New Mexico 87185 and Livermore, California 94550
for the United States Department of Energy
under Contract DE-AC04-94AL85000

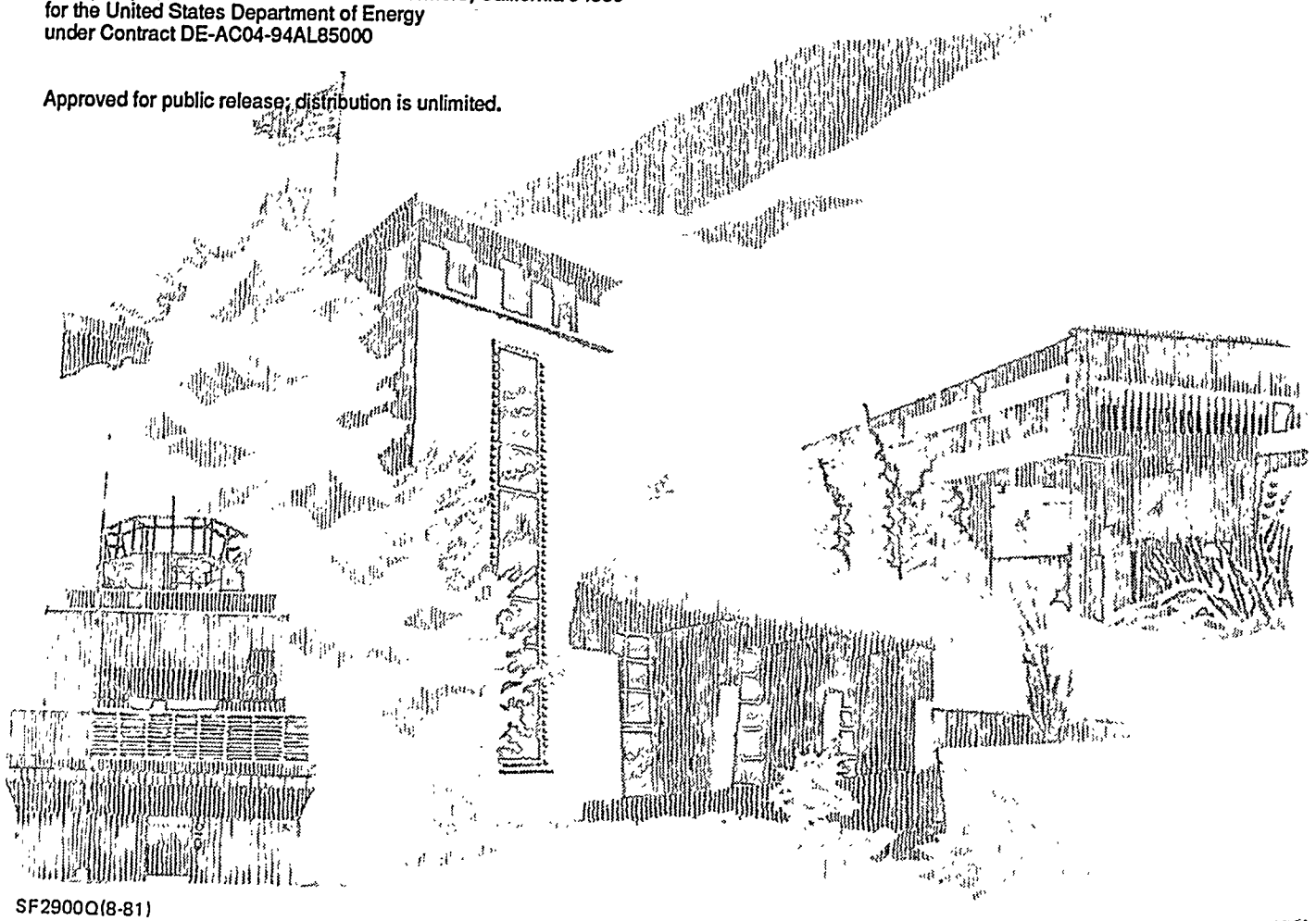

SF2900Q(8-81)

Issued by Sandia National Laboratories, operated for the United States Department of Energy by Sandia Corporation.

Available to DOE and DOE contractors from
Office of Scientific and Technical Information
PO Box 62
Oak Ridge, TN 37831

Prices available from (615) 576-8401, FTS 626-8401

Available to the public from
National Technical Information Service
US Department of Commerce
5285 Port Royal Rd
Springfield, VA 22161

NTIS price codes
Printed copy: A04
Microfiche copy: A01

SAND95-2352
Unlimited Release
Printed December 1995

Distribution
Category UC-704

CHARACTERIZATION OF E-GLASS / POLYESTER WOVEN FABRIC COMPOSITE LAMINATES AND TUBES

T. R. Guess, E. D. Reedy, Jr. and M. E. Stavig

Organic Materials Department 1472
Sandia National Laboratories
Albuquerque, NM 87185

ABSTRACT

This report describes an experimental study that supported the LDRD program *"A General Approach for Analyzing Composite Structures"*. The LDRD was a tightly coupled analytical / experimental effort to develop models for predicting post-yield progressive failure in E-glass fabric/polyester composites subjected to a variety of loading conditions. Elastic properties, fracture toughness parameters, and failure responses were measured on flat laminates, rings and tubes to support the development and validation of material and structural models. Test procedures and results are presented for laminates tested in tension, compression, flexure, short beam shear, double cantilever beam Mode I fracture toughness, and end notched flexure Mode II fracture toughness. Structural responses, including failure, of rings loaded in diametral compression and tubes tested in axial compression, are also documented.

TABLE OF CONTENTS

LIST OF TABLES

LIST OF FIGURES

INTRODUCTION

Potential Sandia programs, such as those addressing crashworthiness, weapon safety, survivability of spacecraft and satellites, armor effectiveness, and the design of lightweight composite structures against failure, require a capability for analyzing the highly nonlinear response of composite materials as they progressively fail under increasing load. In the LDRD study "A General Approach for Analyzing Composite Structures", a general methodology for analyzing the failure of large and complex composite material structures is developed [1-2]. Both in-plane ply failure and ply delamination are modeled. The LDRD study has three main elements: 1) identification of failure modes, appropriate failure criteria, and property degradation relations, 2) development of a methodology for modeling in-plane damage and delamination within the context of a shell element formulation, and 3) assessment of the accuracy of the approach developed.

An extensive experimental program was conducted to generate the necessary data to support the three elements of the LDRD study. A commercially available woven fabric E-glass/polyester composite material system was selected for characterization. This report describes the composite materials and discusses experimental procedures, material response, structural response, and failure modes of flat laminate, ring, and tube specimens.

Approximately 200 individual tests were completed in this study. The volume of data is simply too large to report the results from each and every individual specimen. However, a representative curve that illustrates the typical response from each test type is included. Also, individual data from each set of tests are averaged and these properties are summarized in tabular form.

MATERIALS AND COMPOSITE CONSTRUCTION

Test specimens were machined from laminates (plates) and tubes of E-glass fabric/polyester composite materials. The glass fabric reinforcement used in all materials is a plain weave construction with approximately 5 and 4 rovings per 25 mm in the warp and fill directions, respectively. The fabric meets military specifications MIL-A-46165(MR) for Armor: Woven Glass Roving Fabrics. Individual glass filaments in the fabric have a 68.9 GPa modulus, a density of 2.54 g/cc, and a composition consisting of oxides of silicon, aluminum, calcium, boron, and magnesium fused in an amorphous vitreous state. The polymer matrix is an unsaturated polyester thermoset resin that has a nominal density of 1.2 g/cc. Composite plates and tubes from which specimens are machined were purchased from Russell Plastics Technology Company, Lindenhurst, NY. The materials are divided into two groups, Material 1 and Material 2. Both contain the same glass fabric and polyester resin, but differ in fabrication process and fabric layup. Details of the laminates and tubes from the two materials are listed in Table 1.

MATERIAL 1

Material 1 is a flat laminate ballistic armor material that meets military specifications MIL-A-46166 for Armor: Glass Reinforced Plastic Laminates. Material 1 consists of several layers

(plies) of warp aligned glass fabric. That is, the warp direction of each fabric layer is aligned in the 1-direction of the plate, where the 1- and 2-directions are the principal in-plane axes and the 3-direction is the thickness direction axis of the composite plate. Material 1 laminates are processed using a wet layup, resin impregnation procedure.

Four grades (thicknesses) of Material 1 armor plates (610 mm by 610 mm x thickness) were obtained for the test program. These plates have 7, 12, 21, and 61 fabric layers and nominal thicknesses of 3.4, 6.4, 11.1, and 31.8 mm, respectively. The density of Material 1 is 2.0 g/cc. Microscopy specimens revealed that the Material 1 plates have a the small amount of porosity that is generally located at the interfaces between plies. Microscopy of as-received material indicates some matrix microcracking that probably occurred during the fabrication process. This matrix cracking occurred in each ply and was oriented in the 3-direction (through-the-thickness).

In order to verify the number of fabric plies and to determine the fiber weight fraction in the warp and fill directions, the polyester resin in 6.4 mm thick Material 1 samples was burned off in a 600°C oven. These samples had the expected number of plies (12), with the glass fibers being 74% of the total composite weight (approximately 58% fiber volume). Interestingly, the measured weight ratio of warp fibers to fill fibers is 1.49; whereas, based on the expected weave pattern of 5 rovings per 25 mm width in the warp direction and 4 rovings per 25 mm width in the fill direction, one would expect the weight ratio to be 1.20. Actual counts of roving indicate that there are closer to 5.1 and 3.8 rovings per 25 mm width in the warp and fill directions, respectively; this yields an estimated weight ratio of 1.34, assuming identical size rovings in the warp and fill directions.

It was also observed that Material 1 plates had some wash (skewing) in the plain weave fabric. That is, the warp and fill directions of the fabric are not perfectly aligned with the 1- and 2-directions of the plate. In fact, the angle between the warp and fill direction is not always 90°. This observed wash indicates that the relative values of elastic and strength properties in the 1- and 2-directions will not exactly agree with predictions based on the assumption that the warp and fill reinforcements are orthogonal. The observed wash in the Material 1 laminates is thought to be a by-product of the loose weave of fabric and the wet layup process to fabricate large plates.

MATERIAL 2

In addition to flat laminates, tubular specimens were also required for the LDRD study. The supplier indicated that the wet layup fabrication process was not viable for making the required composite tubes, but tubes could be made using the same E-glass fabric pre-impregnated with the polyester resin. Therefore, tubes and flat laminates fabricated with polyester resin pre-impregnated glass fabric were obtained. Specimens containing prepreg fabric are designated Material 2.

Material 2 Flat Laminates

The orientation of the fabric layers in Material 2 laminates differs from that described previously for material 1. Material 2 laminates contain one or more basic building blocks that

have 6 layers of glass fabric. The two inner layers of each building block are fill aligned, relative to the 1-direction of the plate, and the four outer layers, two on each side, are warp aligned relative to the 1-direction of the plate (see Table 1 notes for more details). Material 2 plates with a 6.4 mm thickness (12 plies) were tested. This material has a density of about 2.1 g/cc and fiber weight fraction of approximately 78% (63% fiber volume).

Material 2 Tubes

Material 2 tubes of 76 mm ID (wall thicknesses of 3.2 and 6.4 mm) and 305 mm ID (wall thicknesses of 6.4 and 12.8 mm) were tested in this study. These tubes were fabricated by winding prepreg fabric around a mandrel and compacting during the cure process. Each fabric layer of the composite is warp aligned in the axial direction of the tube. Some buckling of fabric layers occurred during fabrication, especially in the 305 mm ID tubes.

As noted in Table 1, the densities of Material 2 tubes are significantly lower than the Material 2 laminates. There is considerably more porosity and the tubes appear to be drier than the plates. Accordingly, Material 2 laminate and tube materials cannot be considered to be equivalent. One anticipates that their properties, particularily those influenced by porosity (e.g., interlaminar toughness) to differ considerably.

LAMINATES: TESTS AND RESULTS

A large suite of tests were conducted on specimens machined from the Material 1 and Material 2 flat composite laminates. Table 2 contains a complete listing of the tests types. All tests were performed at ambient conditions of about 22°C and 50% relative humidity. Tests were done either on an Instron 1125 screw-driven load frame or an Instron 8511 electrohydraulic load frame. Instrumentation included strain gages and extensometers. Visual observations and changes in load-deflection responses were used to help determine load at failure initiation, failure locations, and failure modes.

A brief, overall summary of Material 1 and Material 2 laminate properties is given in Table 3. Details of the test procedures and experimental results are discussed in the following sections.

IN-PLANE TENSILE TESTS

In-plane tensile tests include quasi-static (low rate) tests along the principal material axes (1- and 2-directions) and two off-axis orientations (45° and 22.5°) in monotonic loading to failure and in load/unload conditions in which successivel loading cycles are to higher stress levels. In addition there are a few tests at different strain rates.

Testing procedures for all quasi-static tensile tests follow the guidelines in the ASTM Standard Method of Test for Tensile Properties of Plastics (D-638). Specimens are either rectangular (nominal dimensions of 6.3 mm x 25 mm x 250 mm) or flat dogbones with the same overall nominal dimensions. In the reduced-size gage section of the dogbone specimens, the width is 12.7 mm and length is 57 mm. Tensile loads are introduced into the specimens by means

of wedge grips with serrated faces. Specimens are instrumented with a 50-mm extensometer and strain gages in the gage section. Crosshead speed is 2.5 mm/minute.

Material 1 Monotonic Loading

Typical stress-strain responses of Material 1 for monotonic loading in the two principal directions are shown in Figure 1. The 1-direction response is almost linear to failure; whereas, the 2-direction response is nonlinear. The nonlinearity in 2-direction response is a consequence of substantial fabric wash. The fill yarns are not aligned with 2-direction (the warp yarns do align with the 1-direction, 2-direction is orthogonal 1-direction). Elastic, yield and strength properties obtained from the stress strain data are listed in Table 4, along with statistical information and the number of tests.

In order to measure the effect of prior matrix damage on the in-plane stress-strain response, 1-direction tensile tests were done on prestressed specimens. Initially a large specimen (6.4 mm thick x 100 mm wide by 425 mm long) with a 45° fabric warp orientation relative to the specimen longitudinal axis was loaded in an off-axis tension test. The specimen was loaded to 50% of its ultimate strength; rectangular tensile bars were then cut along the warp direction of the large specimen to provide tensile specimens of prestressed material. These specimens have nominal dimensions of 6.4 mm thick x 140 mm length and either 12.8 or 25 mm width. Results are identical for both widths. A typical stress-strain curve for the prestressed material is shown in Figure 1. It can be seen from the curve and the data listed in Table 4 that damage from the prestressing reduces the initial modulus.

Material 1 Load/Unload Results

Tensile tests in which a specimen was successively loaded to higher stress level during load/unload cycles were also performed. Typical load/unload stress-strain responses in the two principal directions are given in Figures 2 and 3. Reductions in initial modulus occur as the specimen is loaded to higher stress levels (and more matrix damage) and can be calculated from the initial slope of the curves. Upon reloading the stress-strain response returns to the state it was prior to the unloading.

Material 1 Off-Axis Tests

Off-axis tensile test specimens were loaded at 45° and 22.5° relative to the 1-direction of Material 1. Typical monotonic loading stress-strain curves are shown in Figure 4; moduli and strength data are listed in Table 4. Shear modulus G_{12} was calculated using procedures in [3]. The off-axis stress-strain responses are highly nonlinear with the initial modulus and yield strength decreasing with increasing off-axis angle. Results of the monotonic off-axis tests are compared with the principal direction data in Figure 5. The 53 Mpa ultimate strength from the 45° off-axis tests was used to define the load level required to condition the prestressed specimens described in the previous section.

Typical load/unload stress-strain responses are shown in Figures 6 and 7. The initial stiffness decreases after unloading from stress levels above the initial yield stress. Upon reloading the stress-strain curve returns to where it was prior to the unloading. The load/unload cycles do not appear to reduce ultimate tensile strength in the off-axis specimens.

Material 2 Monotonic Loading

Material 2 specimens were monotonically loaded in both the 1- and 2-directions, the principal material directions. Recall that the fabric layup of Material 2 differs from that of Material 1. The difference in layer orientation is reflected in material elastic and strength responses. Typical stress-strain responses for Material 2 are shown in Figure 8; elastic and strength properties are listed in Table 4. The responses in the two orthogonal directions are very similar; the curves are nonlinear with initial yield at about 40 Mpa, another yield level around 150 Mpa and failure near 350 Mpa.

Material 1: Effect of Strain Rate

The effect of strain rate on the properties of 1-direction and 45° off-axis specimens was investigated. Monotonic tests were performed at three crosshead speeds (2.5, 610, and 6100 mm/min) on flat dogbone specimens of 3.2 mm thickness. The three crosshead speeds resulted in strain rates of 0.0001 s^{-1}, 0.040 s^{-1} and 0.40 s^{-1} for the 1-direction specimens and 0.0002 s^{-1}, 0.10 s^{-1} and 1.0 s^{-1} for the 45° off-axis specimens. Typical stress-strain responses are shown in Figures 9 and 10; modulus and strength data are listed in Table 5. Over the strain rates tested, there does not appear to be any changes in initial modulus. The strength may be increasing slightly with increasing strain rate.

Failure Modes

The Material 1 specimens loaded in the 1-direction first failed by delamination between layers; delaminations that extended from grip to grip. Final failure was fracture in the grips of outer layers of E-glass fabric. The 2-direction specimens initially failed by matrix cracking, accompanied by yield-like stress-strain behavior. Upon increasing stress, the specimens delaminated axially then failed by fiber breakage in the grips in the same manner as the 1-direction specimens.

The Material 1 off-axis specimens failed by matrix cracking due to shear loading parallel to the off-axis fiber bundles. Large shear deformation was localized (did not extend along the entire gage section) and no fiber breakage was noted.

In Material 2 tension tests, no failure was visually observed until just before failure when the specimen delaminated between layers along the entire specimen length between grips. Obviously there was significant matrix cracking at much lower stresses as evidenced by the nonlinearity in the stress-strain curves.

THICKNESS DIRECTION TENSILE TESTS

The 3-direction (through-the-thickness) tensile strengths were measured for Material 1. Disks of 30 mm diameter were cut from the 6.3, 10.9 and 32 mm thick composite plates. These composite disks were bonded with an epoxy adhesive (about 0.3 mm bond thickness) between two solid aluminum cylinders (30 mm diameter and 38 mm length). Each of the two metal cylinders was pinned through a radial hole to a load train consisting of a clevis and a chain fixture. The specimen were loaded to failure in tension at a crosshead speed of 12.7 mm/min;

strength results are listed in Table 4. Transverse tensile strengths decrease with increasing laminate thickness.

The transverse tensile specimens failed in the resin matrix between fabric layers.

IN-PLANE COMPRESSION TESTS

In-plane compressive response and strength were measured using an IITRI fixture [4, 5]. This fixture is similar to the one described in the ASTM Test for Compressive Properties of Unidirectional or Crossply Fiber Resin Composites (D-3410), except that trapezoidal, rather than conical shaped grips are used. The top and bottom portions of the fixture are aligned by a guidance system which places two parallel roller bushings in the upper half of the fixture and corresponding bushing shafts in the fixture's lower half. Specimens were instrumented with biaxial strain gages which were placed on opposing sides of the 25 mm wide by 152 mm long samples. The specimens, which had a 29 mm gage section, were untabbed and were not supported laterally. An extensometer was used to record crosshead displacement; specimens were loaded at a crosshead speed of 1.3 mm/min.

Material 1 IITRI Tests

A typical IITRI compression stress-strain curve for Material 1 in the 1-direction is shown in Figure 11; elastic and strength data are listed in Table 6. The curves are linear until just prior to specimen failure. Comparison of the elastic data in Tables 4 and 6 shows that the agreement between tension and compression values of moduli and Poisson's ratios in the two directions is quite good. The IITRI compression strengths are lower than the tensile strengths. Because of the observed failure mode (to be discussed later), the measured compression failure strengths are felt to be lower bounds. Data from flexure tests suggest a higher in-plane compression strength than that measured in the IITRI tests.

Material 2 IITRI Tests

Typical IITRI compression stress-strain curves for the 1- and 2-directions for Material 2 are shown in Figure 12; elastic and strength data are listed in Table 6. The compression stress-strain curves are linear to specimen failure. As with Material 1, the agreement between in-plane tension and compression elastic properties is very good. The measured compression strengths are lower bounds because of a buckling failure mode. Figure 13 shows compression stress vs. crosshead displacement responses. This data cannot be used to extract elastic properties, but it illustrates that there is retention of some compression load carrying capacity following the large drop in stress following initial failure. As the displacement is increased, the specimen continues to support a residual compression stress of approximately 20 Mpa.

Failure Modes

Both Material 1 and Material 2 initially failed near the end grips. As the displacement increased there was delamination between layers and the fibers kinked. Material 2 specimens loaded to large displacement as in Figure 13 were tested in tension to measure residual tensile

strength following compression fiber kinking. The residual tensile strength was very low; it ranged between 5 and 12 Mpa.

THICKNESS DIRECTION COMPRESSION TESTS

The 3-direction (through-the-thickness) compression properties were measured for Material 1. Disks of 12.3 mm and 30 mm diameter were cut from the 32 mm thick composite plates. Length-to-diameter ratios of these specimens are 2.4 and 1.1, respectively. These composite disks were loaded in subpress between flat platens. Platen displacement was monitored with an extensometer and specimen strain was taken as the displacement divided by the initial specimen length. Specimens were loaded to failure in compression at a crosshead speed of 2.5 mm/min. A typical stress-strain curve is shown in Figure 14 and modulus and strength results are listed in Table 6. The stress-strain response is essentially linear to failure at about 400 MPa. Note that the 3-direction modulus of 5.6 GPa is much lower than the in-plane moduli because there is no fiber reinforcement in the thickness direction. Identical results were obtained for the two length-to-diameter ratios investigated.

These transverse compression specimens failed in a shearing mode through the fabric layers. The failure shear plane was inclined at 45° to the load axis. Along the shear plane, the glass fibers were broken.

FLEXURE TESTS

Three-point and four-point flexural tests were performed on Material 1 and Material 2 specimens. Testing procedures followed the guidelines in the ASTM Standard Test Methods for Flexural Properties of Plastics and Electrical Insulating Materials (D-790). Test specimens were a nominal 6.4 mm thick, 12.7 mm wide and 150 mm long. The support span was 102 mm for all specimens and the load span was 25 mm for the 4-point bend specimens. Biaxial strain gages were bonded to the tension side of the 3-point bend specimens and to both the tension and compression surfaces of the 4-point flexural specimens. Tests were done at a crosshead speed of 1.3 mm/minute.

Material 1 Flexure Tests

Typical flexural stress-strain responses on the tension surface are shown in Figure 15 for both 3-point and 4-point bend tests on Material 1. Values of elastic and strength properties are listed in Table 6. These curves clearly show that the tension surface elastic responses from both 3- and 4-point bend tests are identical and the maximum tensile stress values are similar. Tension and compression side responses from 4-point flexure tests are plotted in Figure 16. There is little difference in tension and compression behavior.

It is of interest to note from the Figure 16 and Table 6 data that the in-plane 1-direction compression stresses reach values of around 220 MPa. This compression strength is significantly higher than the IITRI compression strength; this is clear evidence that the IITRI compression specimens experienced premature failure.

Comparison of the elastic properties from the flexure tests (Table 6) with the elastic properties from tensile tests (Table 4) reveals that there is excellent agreement between the data from the different test methods.

Material 2 Flexure Tests

Typical flexural stress-strain responses on the tension surface are shown in Figure 17 for both 3-point and 4-point bend tests on Material 2. Values of elastic and strength properties are listed in Table 6. As with Material 1, the tension surface elastic responses from both 3- and 4-point bend tests are identical; the maximum stress values are also the same.

Failure Modes

In both the 3- and 4-point flexure tests, initial failure is generally localized compressive buckling of the fabric layer under or near the load ram on the compression side. With increasing load point displacement, there is delamination between fabric layers with the damage progressing inward with increasing load. Delaminations start out in isolated regions along the layer interfaces then link up as the damage progresses. In the 4-point test, most of the failure occurs between the two load points. In the 3-point test, the damage tends to spread out from the load point. Most delaminations occur on the compression side of specimen mid-thickness, but eventually some delamination of the outer tensile side layers occur.

SHORT BEAM SHEAR (SBS) TESTS

Short beam shear (SBS), 3-point-bend tests with short spans give a measure of a composite's interlaminar shear strength. These tests followed the guidelines in the ASTM Test Method for Apparent Interlaminar Shear Strength of Parallel Fiber Composites by Short Beam Method (D-2344). Tests were done on rectangular bar specimens from Material 1 plates of 6.3, 10.9 and 31.1 mm thickness; specimens were oriented in the 1-direction. Although D-2344 calls only for the measurement of load, in these tests both load and load-point displacement relation were measured. Displacement was monitored with an extensometer attached to the loading ram. Tests were conducted at a crosshead speed of 1.3 mm/min. on specimens at a span-to-depth ratio of 5.0.

Interlaminar shear strengths were measured on as-received material and on specimens with some matrix damage. The purpose of these tests was to determine the effect of prior tensile loading damage on the interlaminar shear strength of Material 1 specimens oriented in the 1-direction. Damage was produced in 580 mm long rectangular bars by loading them in tension to 25%, 50% or 75% of ultimate tensile stress, which corresponds to 129, 259 and 388 MPa, respectively. SBS specimens were then cut from the long prestressed bars and tested in 3-point bending. Additional details of the SBS test series are included in the footnotes of Table 7.

Typical load vs. load-point displacement curves as a function of preload are given for 6.3 mm thickness specimens in Figure 18. The maximum load was used to calculate apparent interlaminar shear strength; results for all specimen sets are listed in Table 7. The Table 7 are plotted in bar graph format in Figure 19. The load-deflection data in Figure 18 clearly shows a decrease in specimen stiffness and maximum load at the 50% and 75% preload conditions. These

results reflect the effect of damage on the interlaminar response of the 6.3 mm thick Material 1 laminate. Note from the Table 7 data that the apparent interlaminar shear strength of undamaged material decreases with increasing specimen thickness. These results follow the trends observed previously in transverse tension tests; namely, that interlaminar strength decreases with increased specimen thickness.

The principal failure mode observed in the SBS tests was delamination between plies near specimen mid-thickness.

FRACTURE TOUGHNESS TESTS

Fracture toughness is a measure of a material's ability to resist crack propagation. Mode I and Mode II critical energy release rates delamination between layers of Material 1 and Material 2 laminates was measured. A double-cantilever-beam (DCB) specimen was used for Mode I (opening mode) tests and an end notched flexure (ENF) specimen for Mode II (shear) tests. Specimen geometry, test procedures, and data reduction techniques for these two tests are discussed in [3].

The edges of all fracture toughness specimens were painted with a thin coating of white correction fluid to enhance visual detection of the crack tip location when it was first produced and during fracture toughness tests. An oil-based correction fluid was thinned with toluene and then brushed onto specimen edges in a thin layer. After drying, additional layers were added as needed to get a smooth opaque coating.

Both the DCB and ENF tests utilize straight sided specimens with a crack on one end. All specimens are 25 mm wide and nominally 6.4 mm thick; the ENF specimens are 125 mm long and the DCB specimens are 230 mm long. A sharp natural crack is required; such a crack was produced by using a thin slitting saw to cut a 0.35 mm wide notch of nominal 30 mm length at specimen mid thickness. This artificial notch was extended as a natural crack by wedging open the notch. The specimen was clamped in a vise to prevent the crack from extending too far while a utility blade was wedged into the notch until the crack extended by 5 to 10 mm. Pencil marks placed on the coating are were to record the position of the crack tip; measurements of crack length were then made with calipers.

End Notch Flexure (ENF) Tests

The purpose of the ENF specimen is to determine G_{IIC}, the critical energy release rate in a pure Mode II (shear) loading. This specimen is reported to produce shear loading at the crack tip without introducing excessive friction between the crack surfaces [3]. A schematic of the ENF specimen is shown in Figure 20. One expression for strain energy release rate, based on elastic beam theory, is given by:

$$G_{IIC} = 9P^2Ca^2 / 2w(2L^3 + 3a^3) \qquad (1)$$

where P is the applied load, C is the compliance, a is the crack length, w is the specimen width and L is the span between the central loading pin and an outer support pin.

The specimen is loaded in a 3-point flexure fixture using a 100 mm support span; the specimen is positioned so that the initial crack length is about 25 mm from one of the support pins. Tests were conducted at a crosshead speed of 2.5 mm/minute with an extensometer measuring load point displacement. A typical curve for Material 2, oriented in the 1-direction is shown in Figure 21. As the load reaches a maximum and begins to decrease, the crack tip has extended inward until it is at specimen mid-thickness under the load pin. During a test, visual observation of the crack tip with a 10X optical microscope was used to detect when the crack tip began to extend. If the load at which the crack extension began was not the maximum load, then the load was noted on the force vs. mid-span deflection response. Note that delamination growth did not occur in an abrupt, unstable way as commonly observed in unidirectional graphite reinforced composites. The experimental compliance was determined from the force-deflection curve; this value along with the force at crack extension and specimen dimensions were inserted in Eq. (1) to calculate G_{IIC}.

ENF test results for Material 1 and Material 2 are listed in Table 8. There is no difference in G_{IIC} values for the 1- and 2-direction specimens. The Mode II fracture toughness of Material 2 is about 25% higher than that of Material 1.

Double Cantilever Beam (DCB) Tests

The purpose of the DCB specimen is to determine the critical energy release rate G_{IC} in Mode I (opening mode) fracture. A schematic of the DCB specimen used in this study is shown in Figure 22. It is a straight sided specimen with a crack at one end. Out-of-plane tension loads are applied to the two beams formed by the crack with hinges that are bonded to the composite specimen with a urethane adhesive. The urethane was used because of its high peel strength; attempts to use an epoxy adhesive were unsuccessful because the hinges tended to peel before a test could be completed.

A typical experimental curve from DCB test on Material 2 is shown in Figure 23. The initial crack length a was first measured; this is the distance from the loading line point to the tip of the starter crack. The specimen was loaded at a crosshead speed of 2.5 mm/min while recording load and load point displacement. The specimen was loaded until the crack extended about 10 mm; extension was visually monitored through a 10X optical microscope. The machine was stopped, the current position of the crack tip marked on the white coating, and then the specimen was unloaded. This procedure was repeated until the crack was approximately 100 mm in length.

The critical strain energy release rate, G_{IC}, is calculated from the compliance and critical load versus crack length data in conjunction with beam theory equations using the data reduction steps described in Reference [3]. From curves like Figure 23, the critical load P_C and specimen compliance C at each crack length a are determined. C vs. a and P_C vs. a are plotted on log-log scales in Figure 24 and Figure 25. In Figure 24 a line of slope +3 is fit to the experimental data for crack lengths greater than 25 mm. The fit is extrapolated to a crack length of 100 mm to determine the compliance C(100). In Figure 25 a line of slope -1 is fit to the P_C vs. a curve to

determine the critical load $P_C(100)$ at a crack length of 100 mm. These two values are used in the following expression to calculate an average value of G_{IC} from the DCB test [3]:

$$G_{IC} = 3A_1A_2^2/2w \qquad (2)$$

where $A_1 = 10^{-6}C(100)$, $A_2 = 102P_C(100)$ and w is the specimen width. The data evaluated in Figures 24 and 25 yields a G_{IC} value of 545 J/m^2.

All DCB tests were performed and the data reduced using the procedures outlined. Results for both Material 1 and Material 2 are listed in Table 8. The Mode I fracture toughness is about 22% higher in Material 1 than in Material 2.

It was also noted that the crack front did not always progress uniformly across the width of the specimen. For that reason, the crack tip location was marked on both sides and the average value used in the data reduction process. In general the crack grew between fabric layers; however, the fracture surface was not a flat, clean surface. The crack followed the contour of the fabric surface and there was significant bridging of fiber between the two fracture surfaces, particularly in the Material 1 specimens. This bridging occurred not only near the crack tip but remained at distances of up to 25 mm behind the tip. The bridging would eventually break when the two loading arms were separated enough to break or pull loose the fibers bridging the gap. The fact that there was significantly less fiber bridging in Material 2 than in Material 1 may account for its lower opening mode fracture toughness.

RINGS AND TUBES: TESTS AND RESULTS

Material 2 rings were tested in diametral compression and Material 2 tubes were tested in axial compression. Table 9 lists the matrix of tests performed in this study. These tests measured structural response and illustrated the progression of failure. Rings of 78 and 305 mm inside diameter and various wall thicknesses of 3.2, 6.4 and 12.8 mm were loaded in diametral compression. Tubes of 78 mm inner diameter with thicknesses of 3.2 mm and 6.4 mm were tested in axial compression.

DIAMETRAL COMPRESSION TESTS ON RINGS

Load-deflection curves in the elastic, post-yield, and failure regions were obtained for composite rings loaded in diametral compression between flat platens. Delamination between plies and the development of hinge points when the laminate failed in flexure were the principal failure modes. Even with many delaminations at large deflections, composite rings continued to carry load and retain some structural integrity.

Load-Deflection Response

The experimental setup and the location of strain gages on composite rings loaded in diametral compression are shown in Figure 26. Ring deflection was measured with an

extensometer attached to the loading platens, and hoop and axial strains were monitored with biaxial strain gages. Typical load vs. load point deflection responses are shown in Figures 27 and 28 for rings of 78 mm ID and 305 mm ID, respectively; data for individual specimens are listed in Table 10. Figure 27 shows curves up to 58 mm deflection for 25 mm wide rings and Figure 28 has curves up to 200 mm deflection for 64 mm wide rings.

Elastic Response

Reference [6] contains formulas for the moments and deflections of circular rings subjected to diametral compressive loading. These equations are for isotropic materials and for small deflections. They were reformulated to a form that is applicable for calculating the hoop modulus using the initial slope of a load-deflection curve and ring dimensions. The equation is

$$E_{hoop} = (1.788R^3/wt^3)(P/d) \qquad (3)$$

where Ehoop is the hoop direction modulus of elasticity, R is the mean radius of the ring, P is the load, d is the deflection, w is the width, and t is the thickness. Equation (3) was used to calculate the hoop moduli of the test rings. These values are listed in Table 10 along with Poisson ratio values obtained from strain gage data.

Failure Modes

Typical examples of the progressive failure that occurred in the composite rings during diametral compression tests are shown in Figures 29 and 30. There are photographs of 305 mm ID rings of taken at different levels of deflection. The principal failure mode is delamination between plies. This mode is readily apparent at the 0° and 180° locations. A series of delaminations that linked to produce circumferential cracks near mid-thickness are present even though they are difficult to see in Figures 29 and 30. In most rings, the delaminations that produced the circumferential cracks appeared to initiate first at the 0° and 180° locations, then at 225° , or 315° locations. Even though there were many delaminations at large deflections, the composite rings continued to carry significant loads.

AXIAL COMPRESSION

Load-deflection curves and experimental values of initial axial modulus, peak loads and loads at 25 mm deflection were obtained for composite tubes loaded in axial compression.

Test Setup and Results

The experimental setup for Material 2 composite tubes (78 mm ID) loaded in axial compression is shown in Figure 31; specimen lengths and thicknesses are listed in Table 11 along with some of the experimental results. Specimens were machined either with or without a 45° external chamfer at the top of the tube. Those with no chamfer were used primarily to measure axial modulus. The purpose of the chamfer on the other specimens was to trigger stable progressive crushing of the tube. Total axial deformation was measured with an extensometer

attached to the load platens; hoop and axial strains were monitored with strain gages located at midlength of the specimen.

Typical load-displacement responses of tubes with chamfered ends are shown in Figures 32 and 33. The loading platens for specimens that yielded the Figure 32 curves were flat. In these tests, radial deformation of the composite during axial crush is both inward and outward. The platen loading the chamfered end of the Figure 33 specimens has an internal plug (see Figure 31) that forces all radial deformation to be outward.

Failure Modes

Typical examples of progressive failure that occurred in the composite rings during axial compression tests are shown in Figures 34 and 35. These are photographs of tubes (wall thicknesses of 3.2 and 6.4 mm) taken at increasing deflection levels. In general failure initiates at the chamfer and then to crush zone progresses downward as the deflection increases; specifics for individual specimens are noted in Table 11. For specimens loaded with flat platens, the composite tube tends to delaminate at mid-thickness and is forced open by a wedge of crushed material at this location. The remainder of the materials then peels off radially; some inward and some outward. It is evident that delamination, flexure, tensile, and compressive failure modes are all generated simultaneously during crush.

There were differences in response for those tubes loaded with the platen having an internal plug with a 6 mm radius at the lip that forced all radial displacement outward. The OD of the plug was a slip fit into the ID of the tube. As crush begins and material moves, the fit of the plug most likely becomes an interference fit because it was very difficult to remove the plug at the end of a test. This friction may account for the higher loads required to crush 6.4 mm tubes when the platen with a plug was used (see data in Figures 32 and 33 and in Table 11). The reason the 3.2 mm thick tubes have lower crush strengths when the plug is used is not known.

Note in Figures 32 and 33 that the tubes continue to maintain significant load carrying capacity as they progressively crush.

SUMMARY

This report describes an experimental study that supported the LDRD program "A General Approach for Analyzing Composite Structures". The LDRD was a tightly coupled analytical/experimental effort to develop models for predicting post-yield progressive failure in E-glass fabric/polyester composites subjected to a variety of loading conditions. Elastic properties, fracture toughness parameters, and failure responses were measured on flat laminates, rings and tubes to support the development and validation of material and structural models. Test procedures and results were presented for laminates tested in tension, compression, flexure, short beam shear, double cantilever beam Mode I fracture toughness, and end notched flexure Mode II fracture toughness. Flat samples were tested for elastic properties, post-yield behavior and strengths. Load-displacement and load-strain curves in the elastic, post-yield, and failure regions were obtained from diametral compression tests on composite rings and axial compression on tubes. Delamination between plies was the principal failure mode observed in the diametral

compression tests. The composite rings retained some structural integrity at large deflections following multiple delaminations.

In conclusion, a large body of experimental data has been generated on the mechanical properties and structural response of E-glass fabric/polyester composite plates, rings, and tubes in support of the LDRD program. This data base provides experimental information to assist in the development of material and finite element models for predicting the post-yield response of composite structures.

ACKNOWLEDGMENTS

John Totten and Wendell Kawahara conducted the high strain rate tests for Material 1. Adra Baca and David Lo reviewed and commented on the original manuscript.

REFERENCES

[1] Dunn, M. L., Reedy, E. D., and Guess, T. R., "*Delamination of Woven E-Glass Fabric Composites,*" proceedings of the 39th International SAMPE Symposium, April 11-14,1994, Anaheim, CA.

[2] Reedy, Jr., E. D., Mello, F. J., and Guess, T. R., "*Modeling the Initiation and Growth of Delamination in Composite Structures*," SAND95-3670, Sandia National Laboratories, January 1996.

[3] Carlsson, L. A., and Pipes, R. B., Experimental Characterization of Advance Composite Materials, Prentice-Hall, Inc., New Jersey, 1987, pp. 62-64 and 160-170.

[4] Adsit, N. R., "*Compression Testing of Graphite/Epoxy*," Compression Testing of Homogeneous Materials and Composites, ASTM STP 808, Richard Chait and Ralph Papirno, Eds., American Society of Testing and Materials, 1983, pp. 175-186.

[5] Hofer, K. E., Jr., and Rao, P. N., "*A New Static Compression Fixture for Advanced Composite Materials*," Journal of Testing and Evaluation , JTEVA, Vol. 5, No. 4, July 1977, pp. 278-283.

[6] Roark, R. J., and Young, W. C., Formulas for Stress and Strain, fifth edition, McGraw-Hill Book Company, New York, 1975, p. 220.

Table 1. Description of Laminates and Tubes Used in Test Program.

FLAT PLATES			
Russell Designation	**Number of Plies**	**Nominal Thickness (mm)**	**Density (g/cc)**
	MATERIAL 1		
Grade 1	7	3.2	2.0
Grade 2	12	6.3	2.0
Grade 4	21	10.9	
Grade 5	61	31.8	
	MATERIAL 2		
---	12	6.4	2.08

TUBES			
Tube Inside Dia. (mm)	**Number of Plies**	**Wall Thickness (mm)**	**Density (g/cc)**
	MATERIAL 2		
78		3.2	1.75
78		6.4	1.90
305		6.4	1.72
305		12.8	1.57

Notes:

Reinforcement: E-glass woven fabric per military specification MIL-A-46165(MR). Approximately fFive rovings (yarn ends) and 3.7 rovings per inch width in the fabric warp and fill directions, respectively.

Resin Matrix: Polyester

Material 1 Composite (Russell Plastics ballistic armor per military specification MIL-A-46166):

- Flat laminate of multiple plies (layers) of fabric
- Wet layup fabrication process.
- Fabric orientation-- warp rovings of all plies oriented in 1-direction and fill rovings in the 2-direction of laminate. The 1- and 2-directions are inplane orthogonal directions (0 and 90 degrees) and the 3-direction is normal (transverse) to the laminate.

Material 2 Flat Laminates

- Prepreg fabric used in fabrication process.
- Fabric orientation and layup--The warp direction of the prepreg plies are stacked in a $[0\backslash0\backslash90\backslash90\backslash0\backslash0]_2$ orientation where 0 is in the 1-direction and 90 in the 2-direction of the laminate. There are two repeat patterns as denoted by the subscript 2; the Material 2 laminates are 12 plies thick.

Material 2 Tubes

- Prepreg fabric wrapped around a cylindrical mandrel in fabrication process.
- Fabric orientation and layup--The warp direction of each prepreg ply is oriented in the tube axial direction and the fill direction in the tube hoop direction.

Table 2. Test Matrix for Material 1 and Material 2 Laminate Specimens.

TYPE OF TEST	MATERIAL 1 Loading		MATERIAL 2 Loading
	Monotonic	Load/Unload	Monotonic
IN-PLANE TENSION			
1-Direction	X	X	X
1-Direction at High Strain Rates	X		
1- Direction (Following Prestress)	X		
2-Direction	X	X	X
45° Off-Axis	X	X	
45° Off-Axis at High Strain Rates	X		
22.5° Off-Axis	X	X	
TRANSVERSE TENSION (3-Dir)	X		
IN-PLANE (IITRI) COMPRESSION			
1-Direction	X		X
2-Direction			X
TRANSVERSE COMPRESSION (3-Dir.)	X		
3-POINT FLEXURE			
1-Direction	X		X
2-Direction	X		X
4-POINT FLEXURE			
1-Direction	X		X
2-Direction	X		X
SHORT BEAM SHEAR (SBS)			
0% Tensile Preload	X		
25% Tensile Preload	X		
50% Tensile Preload	X		
75% Tensile Preload	X		
DCB Mode I FRACTURE TOUGHNESS			
1-Direction	X		X
2-Direction	X		X
ENF Mode II FRACTURE TOUGHNESS			
1-Direction	X		X
2-Direction	X		X

Notes:

1. Material 1 is an E-glass fabric/polyester wet layup composite with warp direction of each layer oriented in the same direction (1-direction of plate).
2. Material 2 is an E-glass fabric/polyester prepreg composite. See Table1 for the fabric layup. Outer ply fabric warp direction is oriented in the 1-direction of the composite plate.
3. Test specimen longitudinal axis relative to 1-2 axes of composite plate.

Table 3. Summary of Laminate Properties

PROPERTY	MATERIAL 1 (Wet Layup Fabrication)		MATERIAL 2 (Prepreg Fabrication)	
	1-Direction	2-Direction[1]	1-Direction	2-Direction
DENSITY (g/cc)	2.0	2.0	2.1	2.1
TENSION				
Initial Modulus (GPa)	28.6	16.0 to 17.6	32.1	27.3
Secondary Modulus (GPa)	---	5.9	23.0	21.4
Poisson's Ratio	0.08	0.06	0.14	0.12
Yield Stress (MPa)	---	76	36	42
Failure Stress (MPa)	516	168 to 254	332	367
COMPRESSION				
Initial Modulus (GPa)	27.8	19.9	31.6	28.5
Poisson's Ratio	0.07	---	0.11	0.11
Failure Stress (MPa)	122	82	170	169
FLEXURE				
4-Point				
Initial Modulus (GPa)				
-Tension side	27.6	16.4	29.7	---
-Compression side	27.6	17.2	30.1	---
Poisson's Ratio	---	0.09	0.13	---
Maximum Stress (GPa)	211	127	250	---
3-Point				
Initial Modulus (GPa)	27.7	17.2 to 18.1	31.3	---
Maximum Stress (GPa)	217	138 to 149	248	---
FRACTURE TOUGHNESS				
DCB Mode I G_{IC} (J/m^2)	722	696	579	---
ENF Mode II G_{IIC} (J/m^2)	449	455	567	---

[1] The fill rovings of the Material 1 fabric were not always aligned with the 2-direction of the plate. This fabric wash resulted in a range of properties for the 2-direction specimens. Therefore, these 2-direction properties are not exactly representative of fill directed properties.

Table 4. Tensile Test Results for Material 1 and Material 2 Laminates

TENSILE PROPERTY	MATERIAL 1				MATERIAL 2			
	N	Avg.	StDev	cv (%)	N	Avg.	StDev	cv (%)
1-Direction								
E_1 (GPa)	8	**28.6**	1.7	6.1	3	**32.1**	0.47	1.5
E_1^S (GPa)	--	--	--	--	3	**23.0**	1.1	4.9
ν_{12}	4	**0.08**	0.008	10.2	3	**0.14**	0.01	3.8
F_1^Y (MPa)	--	--	--	--	3	**36**	1.7	4.8
F_1 (MPa)	8	**516**	21.0	4.1	3	**332**	27.5	8.3
1-Direction Following Pre-Stress								
E_1 (GPa)	6	**26.8**	0.7	2.5	--	--	--	--
ν_{12}	5	**0.072**	0.014	19.6	--	--	--	--
F_1 (MPa)	6	**372**	17.5	4.7	--	--	--	--
2-Direction								
E_2 (GPa)	6	**16.0**	0.6	3.8	3	**27.3**	.42	1.5
E_2^S (GPa)	--	**5.9**	--	--	3	**21.4**	0.80	3.8
ν_{21}	3	**0.06**	0.006	9.5	3	**0.12**	0.004	3.0
F_2^Y (MPa)	6	**75.8**	4.7	6.2	3	**42**	4.0	9.6
F_2 (MPa)	6	**168**	2.4	1.4	3	**367**	7.6	2.1
In-Plane Off-Axis								
$E_{22.5°}$ (GPa)	8	**16.3**	0.6	3.5	--	--	--	--
$\nu_{22.5°}$	1	**0.47**	--	--	--	--	--	--
$F_{22.5°}$ (MPa)	7	**78.3**	4.7	6.0	--	--	--	--
$E_{45°}$ (GPa)	6	**13.1**	1.24	9.5	--	--	--	--
$\nu_{45°}$	2	**0.53**	--	--	--	--	--	--
$F_{45°}$ (MPa)	6	**52.7**	1.0	2.0	--	--	--	--
G_{12} (MPa)	--	**3.8**	--	--				
3-Direction (Transverse)								
F_3 (MPa)								
t= 6.3 mm	4	**5.8**	0.58	10.0	--	--	--	--
t= 10.9 mm	3	**2.3**	0.24	10.9	--	--	--	--
t= 32 mm	3	**2.0**	0.28	14.3	--	--	--	--

Notes:

1. E, ν and F denote modulus, Poisson's ratio and strength, respectively. The subscripts1 & 2 represent the 1 and 2 directions of the material and the subscripts 22.5° and 45° indicate the angle of loading with respect to the 1-direction. The superscripts S and Y represent secondary slope and yield strength.
2. Crosshead speed is 2.5 mm/min for these tensile tests; specimen thickness is about 6.3 mm except for some transverse tests.
3. N, Avg., StDev., and cv are the number of specimens, the average, the standard deviation and the coefficient of variation, respectively.
4. All specimens are rectangular bars except for the Material 1, 1-direction specimens which are dogbone shaped.

Table 5. Material 1 Tensile Properties as a Function of Strain Rate.

STRAIN RATE (s^{-1})	INITIAL MODULUS (GPa)				ULTIMATE STRENGTH (MPa)			
	N	Avg.	StDev	cv (%)	N	Avg.	StDev	cv (%)
			1-DIRECTION					
0.00010	1	**27.3**	--	--	1	**410**	--	--
0.040	3	**27.3**	0.6	2.1	3	**446**	31	7.0
0.40	4	**27.3**	1.5	5.6	4	**487**	49	10.2
			45° - DIIRECTION					
0.00020	1	**10.7**	--	--	1	**45.3**	--	--
0.10	2	**11.2**	0.07	0.6	2	**44.4**	2.1	4.7
1.0	2	**11.1**	1.1	10.2	2	**51.8**	6.4	12.4

Notes:
1. In-plane tensile tests on Material 1 dogbone shaped specimens of nominal 3.2 mm thickness.
2. N, Avg., StDev., and cv are the number of specimens, the average, the standard devialtion and the coefficient of variation, respectively,

Table 6. Compression and Flexural Results for Material 1 and Material 2 Laminates.

PROPERTY	MATERIAL 1				MATERIAL 2			
	N	Avg.	StDev	cv (%)	N	Avg.	StDev	cv (%)
COMPRESSION								
1-Direction								
E_1 (GPa)	3	**27.8**	1.7	6.2	3	**31.6**	1.1	3.5
ν_{12}	3	**0.06**	0.005	9.1	3	**0.11**	0.005	4.5
F_1 (MPa)	3	**122**	18.4	15.0	3	**170**	17.6	10.4
F_1 residual (MPa)	--	--	--	--	3	**18.3**	1.5	8.2
2-Direction								
E_2 (GPa)	--	--	--	--	3	**28.5**	0.90	3.2
ν_{21}	--	--	--	--	3	**0.11**	0.10	9.1
F_2 (MPa)	--	--	--	--	3	**169**	3.6	2.1
F_2 residual (MPa)	--	--	--	--	3	**16.7**	2.9	17.4
3-Direction (Transverse)								
E_2 (GPa)	5	**5.6**	0.42	7.5	--	--	--	--
F_3 (MPa)	5	**400**	38.2	9.5	--	--	--	--
3-POINT FLEXURE								
E_1 (GPa)	3	**27.7**	2.4	8.5	2	**31.3**	--	--
E_2 (GPa)	3	**17.2**	0.90	5.4	--	--	--	--
F_1 (MPa)	2	**217**	2.4	1.0	2	**248**	--	--
F_2 (MPa)	3	**149**	1.8	1.4	--	--	--	--
4-POINT FLEXURE								
E_1 (tension side), (GPa)	6	**27.6**	0.5	1.7	1	**29.7**	--	--
E_1 comp. side), ($Gpa_)$)	6	**27.6**	0.8	3.0	1	**30.1**	--	--
E_2 (tension side), (GPa)	3	**16.4**	0.60	3.6	--	--	--	--
E_2 comp. side), (GPa)	3	**17.2**	0.20	1.2	--	--	--	--
ν_{12}	--	--	--	--	1	**0.13**	--	--
F_1 (MPa)	6	**211**	19.9	9.5	2	**250**	--	--
F_2 (MPa)	3	**127**	9.0	7.1	--	--	--	--

Notes:

1. Flexural tests support span = 76 mm and load span = 25.4 mm for 4-point flax tests.
2. E, n and F denote modulus, Poisson's ratio and strength, respectively. The subscripts 1, 2 & 3 represent the 1 and 2 in-plane , and 3 (transverse) directions of the material.
3. N, Avg., StDev., and cv are the number of specimens, the average, the standard devialtion and the coefficient of variation, respectively,
3. All inplane test specimen are about 6.4 mm thick.
4. Residual strength of inplane compression tests is the average stress carried by specimen at large displacements.

Table 7. Short Beam Shear (SBS) Interlaminar Strengths for Material 1 Laminates

SPECIMEN THICKNESS (mm)	SPECIMEN WIDTH (mm)	TENSILE PRELOAD (%)	NUMBER TESTS	INTERLAMINAR SHEAR STRENGTH		
				Average (MPa)	StDev. (MPa)	cv (%)
6.3	6.4	0	11	**13.5**	0.7	5.4
6.3	12.7	0	11	**13.7**	1.0	7.1
6.3	12.7	25	10	**14.7**	0.2	1.4
6.3	12.7	50	10	**11.9**	0.4	3.7
6.3	12.7	75	5	**7.4**	1.0	13.7
10.9	10.1	0	5	**9.2**	0.2	2.3
10.9	10.1	25	5	**7.3**	0.3	4.0
10.9	10.1	50	5	----	----	----
31.1	32.0	0	10	**8.3**	0.7	7.9

Notes:
1. Specimen longitudinal axis parallel to 1-direction (warp) of Material 1 plates.
2. Tests at a crosshead speed of 1.3 mm/minute.
3. Specimen span to thickness ratio = l/t = 5.0.
4. Radii of supports and load ram = t/4 and t/2, respectively; t is the specimen thickness.
5. Tensile Preload Specimens: 500 mm long bars pre-stressed by of inplane tensile loading (to percentage of failure stress). Long bars then cut into shorter samples for short beam shear (SBS) tests. The 31.1 mm thick material was too thick to grip for preloading; the 10.9 mm thick specimens were so damaged by 50% tensile preload that the SBS specimens failed by crushing rather than by delamination.
6. For specimens with no preload, initial failure in SBS tests is shear delamination near midplane with no apparent surface damage prior to 1st failure.
7. StDev is the standard deviation and cv is the coefficient of variation (StDev divided by the Average).

Table 8. Double Cantilever (DCB) and End Notched Flexure (ENF) Fracture Toughness Results for Material 1 and Material 2 Laminates.

TEST	MATERIAL 1				MATERIAL 2			
	N	Avg.	StDev	cv (%)	N	Avg.	StDev	cv (%)
DOUBLE CANTILEVER BEAM								
1-Direction								
G_{IC} (J/m^2)	2	**722**	24	3.3	3	**579**	30	5.2
2-Direction								
G_{IC} (J/m^2)	5	**696**	59	8.5	--	--	--	--
END NOTCH FLEXURE								
1-Direction								
G_{IIC} (J/m^2)	2	**449**	52	11.7	3	**567**	37	6.4
2-Direction	6	**455**	52	11.4	--	--	--	--
G_{IIC} (J/m^2)								

Notes:

1. G is the energy release rate for crack extension and the subscripts IC and IIC denote the critical toughness values for Mode I and Mode II, respectively.
2. N, Avg., StDev., and cv are the number of specimens, the average, the standard deviation and the coefficient of variation, respectively.
3. All specimens are slotted rectangular bars; specimen thickness is about 6.3.

Table 9. Test Matrix for Material 2 Ring and Tube Specimens

TYPE OF TEST	RINGS AND TUBES WALL THICKNESSES		
	3.2 mm	6.4 mm	12.8 mm
DIAMETRAL COMPRESSION OF RINGS			
Inside Diameter = 78 mm	X	X	
Inside Diameter = 305 mm		X	X
AXIAL COMPRESSION OF TUBES (ID = 78 mm)			
Tubes with one champered end			
-Loaded with flat platens	X	X	
-Loaded with inner plug on one end	X	X	
Tubes with no champer			
-Loaded with flat platens	X	X	

Notes:

1. Material 2 is an E-glass fabric/polyester prepreg composite. Fabric warp direction is oriented in the axial direction of the composite rings and tubes.

Table 10. Diametral Compression Test Results for Material 2 Rings.

SPEC. ID	DC3-E1	DC3-E2	DC3-E3	DC3-Q1	DC3-Q2	DC3-Q3
WEIGHT (gm)	35.35	36.39	35.99	72.17	72.64	---
DENSITY (gm/cc)	1.71	1.76	1.69	1.88	1.97	---
LENGTH, L (mm)	25.15	25.91	25.40	25.15	25.40	25.40
ID (mm)	77.98	77.85	77.85	77.95	77.85	77.85
OD (mm)	84.42	84.14	84.43	89.54	88.93	88.76
THICKNESS, T (mm)	3.22	3.14	3.29	5.79	5.54	5.45
MEAN RADIUS, R mm)	40.65	40.53	40.58	42.03	41.76	41.80
P/DEL (N/mm) (Experimental)	87.6	96.1	93.7	651.4	604.1	665.4
$E=(1.788*R^3/L*T^3)*P/DEL$ (GPa)	12.5	14.2	12.4	17.7	18.3	21.1
POISSON'S RATIO($\nu_{hoop\text{-}axial}$)	---	---	---	0.13	---	---

SPEC. ID	DC12-Q1	DC12-Q2	DC12-Q3	DC12-H1	DC12-H2	DC12-H3
WEIGHT (gm)	683	683	681	1295	1288	1285
DENSITY (gm/cc)	1.68	1.78	1.70	1.63	1.56	1.53
LENGTH, L (mm)	63.83	63.80	63.88	65.41	65.58	65.48
ID (mm)	305.7	305.7	305.7	305.3	305.9	305.8
OD (mm)	318.7	318.0	318.5	330.5	331.1	331.3
THICKNESS, T (mm)	6.52	6.14	6.40	12.12	12.59	12.80
MEAN RADIUS, R mm)	156.11	155.91	156.07	159.18	159.24	159.27
P/DEL (N/mm) (Experimental)	267	303	323	1555	1830	1790
$E=(1.788*R^3/L*T^3)*P/DEL$ (GPa)	18.03	24.36	22.97	16.90	17.71	16.50
POISSON'S RATIO ($\nu_{hoop\text{-}axial}$)	0.072	.070 /.096	---	---	0.10	---

Table 11. Axial Compression Tests for Material 2 Tubes.

SPECIMEN ID	NOMINAL THICKNESS (mm)	TUBE LENGTH (mm)	CROSS-HEAD SPEED (mm/minute)	TOP PLATEN WITH PLUG	INITIAL MODULUS (GPa)	1st PEAK LOAD (N)	LOAD @ 25 mm DISPL. (N)	COMMENTS
			TUBES WITH ENDS FLAT					
AC3-E1	3.2	77	6.4	NO	24.0	60,600	23,400*	Test stopped after less than
AC3-Q1	6.4	77	2.5	NO	25.2	---	---	Stopped test at 89,000 N load.
AC3-Q1B	6.4	77	6.4	NO	21.0	149,000	51,000**	2nd loading of specimen AC3_Q1
AC3-Q2	6.4	77	6.4	NO	24.8	---	---	Modulus measurement only.
			TUBES WITH 45°CHAMFER ON ONE END					
RTUBE2-1	3.2	142	12.7	NO	---	45,000	32,000	Crush on chamfer end; material moved radially in and out.
RTUBE2-2	3.2	142	12.7	NO	---	35,000	26,000	Crush on chamfer end; material moved radially in and out.
RTUBE2-3	3.2	142	12.7	NO	---	45,000	37,000	Crush on chamfer end; material moved radially in and out.
RTUBE2-4	3.2	142	12.7	YES	25.5	20,500	22,000	Crush on chamfer end; material moved radially outward
RTUBE2-5	3.2	142	12.7	YES	25.2	18,000	19,000	
RTUBE1-1	6.4	142	12.7	NO	---	59,000	64,000	Crush on chamfer end; material moved radially in and out.
RTUBE1-2	6.4	142	12.7	NO	---	47,000	50,000	Crush on chamfer end; material moved radially in and out.
RTUBE1-3	6.4	142	12.7	NO	---	52,000	46,000	Crush on chamfer end; material moved radially in and out.
RTUBE1-4	6.4	142	12.7	YES	---	84,500	---	ICrush on chamfer end; no data after 12 mm displacemtent.
RTUBE1-5	6.4	142	12.7	YES	21.4	87,000	50,000	Initially crushed on chamfer end; then broomed on other end.
RTUBE1-6	6.4	142	12.7	YES	21.5	73,000	88,000	Crush on chamfer end; some buckling below end of plug.
RTUBE1-7	6.4	142	12.7	YES	24.1	90,000	80,000	Crush on chamfer end; some buckling below end of plug.

* Load at 1.3 mm displacement
** Load at 11 mm displacement

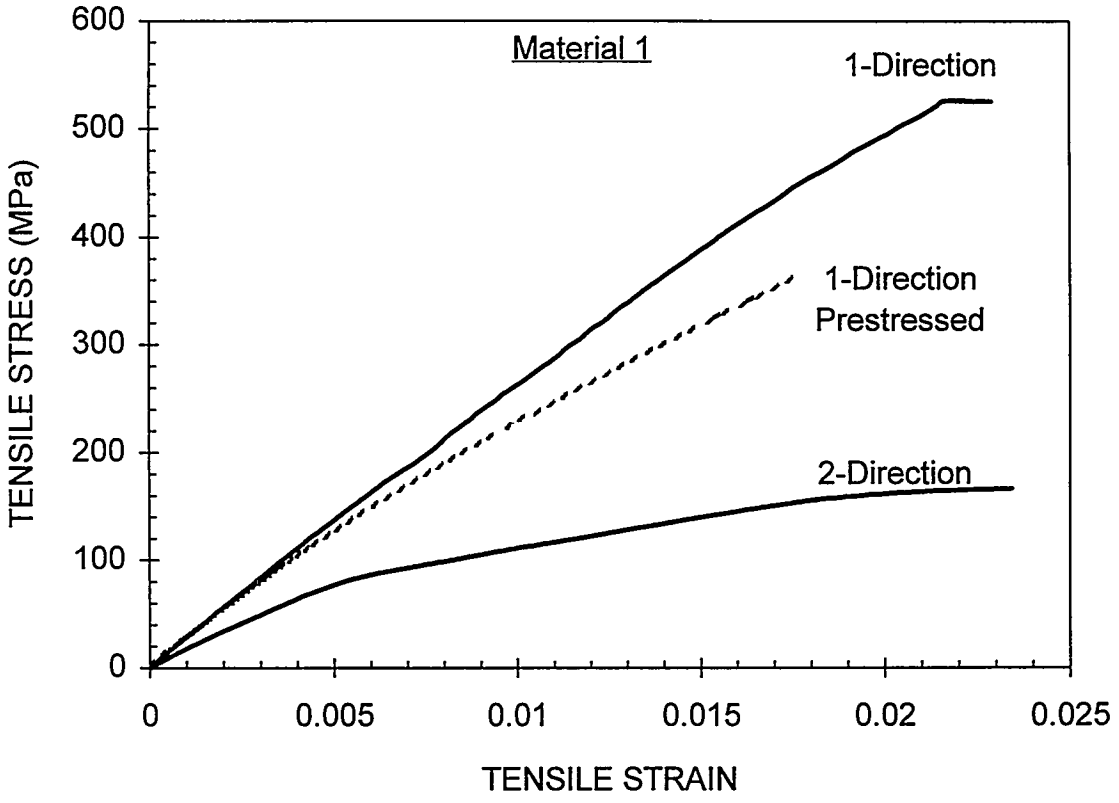

Fig. 1. Typical in-plane tensile stress-strain responses of Material 1 for monotonic loading in the laminate principal directions. Prestressed specimen loaded to 50% of ultimate in ±45° direction prior to cutting out tensile specimen testing in 1-direction.

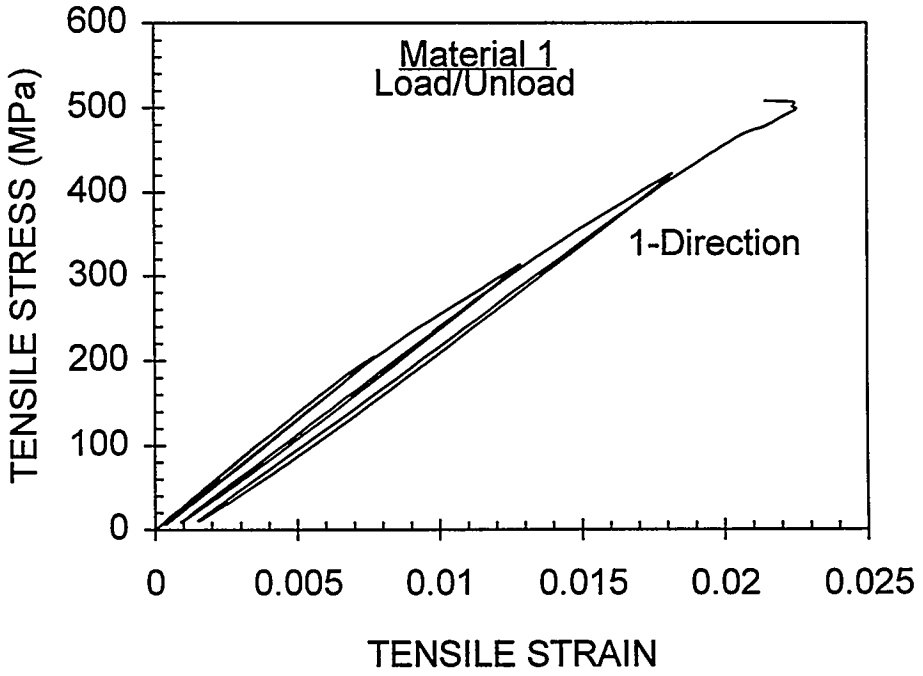

Fig. 2. Typical load/unload stress-strain response for Material 1 tested in the 1-direction. Successive load/unload cycles taken to higher stress levels.

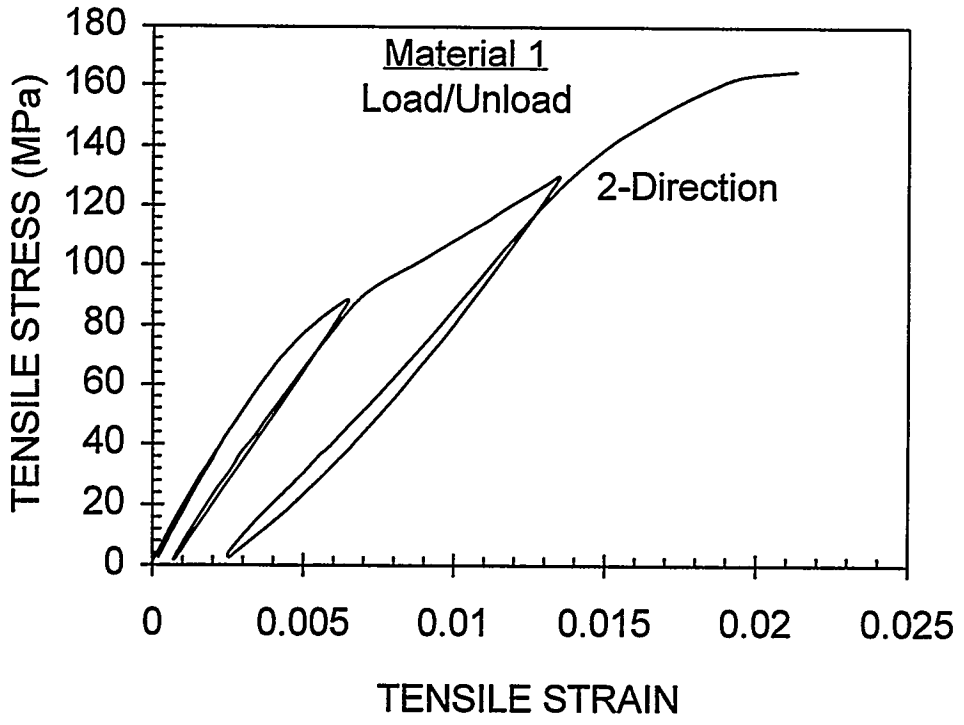

Fig. 3. Typical load/unload stress-strain response for Material 1 tested in the 2-direction. Successive load/unload cycles taken to higher stress levels.

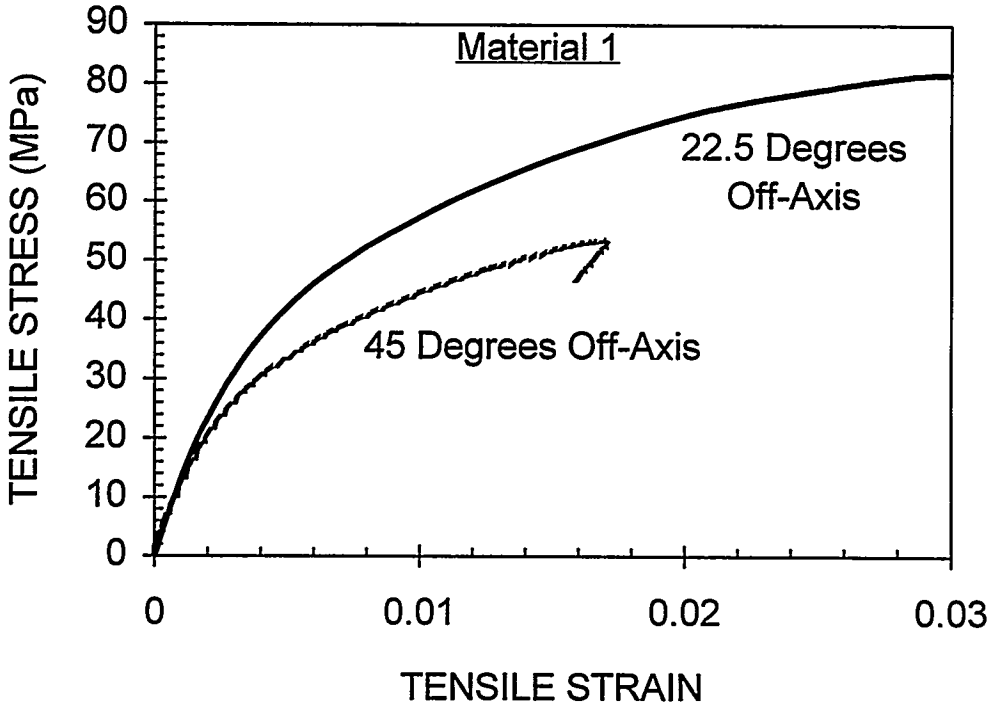

Fig. 4. Typical in-plane off-axis tensile stress-strain responses of Material 1 for monotonic loading at 22.5° and 45° relative to the laminate 1-direction.

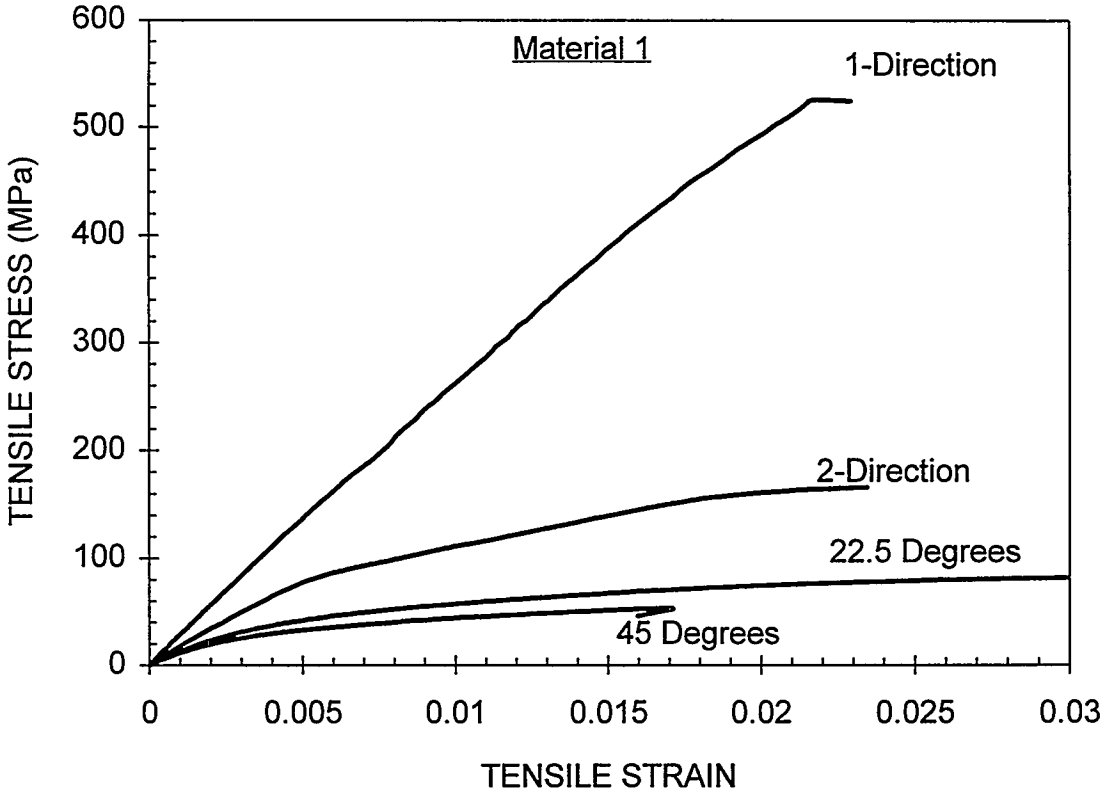

Fig. 5. Summary plot of in-plane tensile stress-strain responses of Material 1 for monotonic loading in four directions.

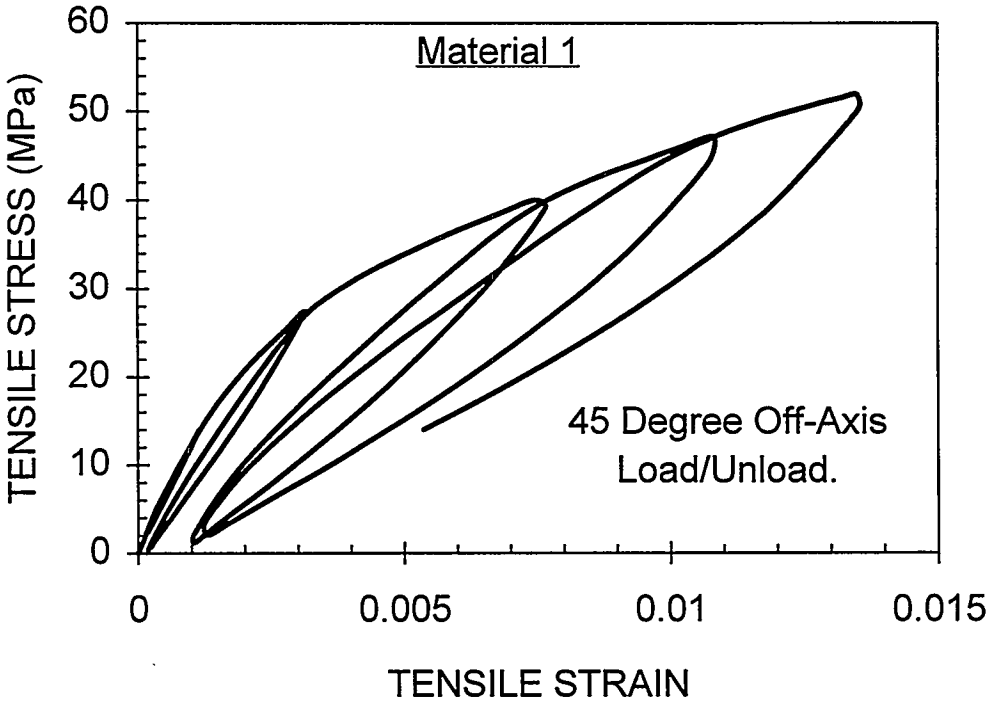

Fig. 6. Typical load/unload stress-strain response for Material 1 tested in 45° off-axis tension. Successive load/unload cycles taken to higher stress levels.

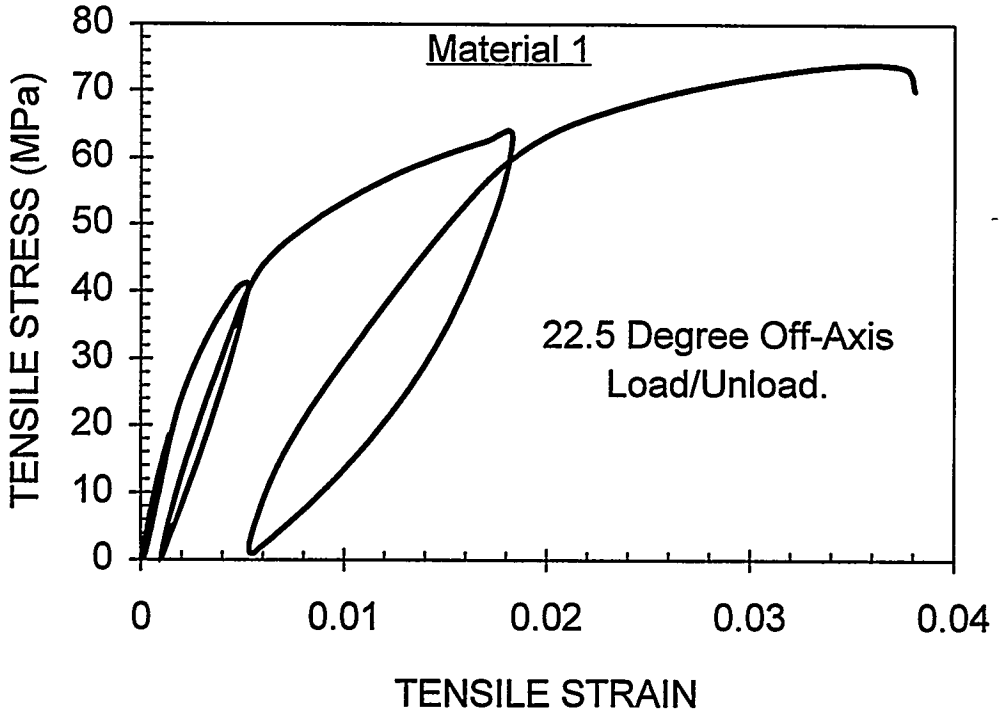

Fig. 7. Typical load/unload stress-strain response for Material 1 tested in the 22.5° off-axis tension. Successive load/unload cycles taken to higher stress levels.

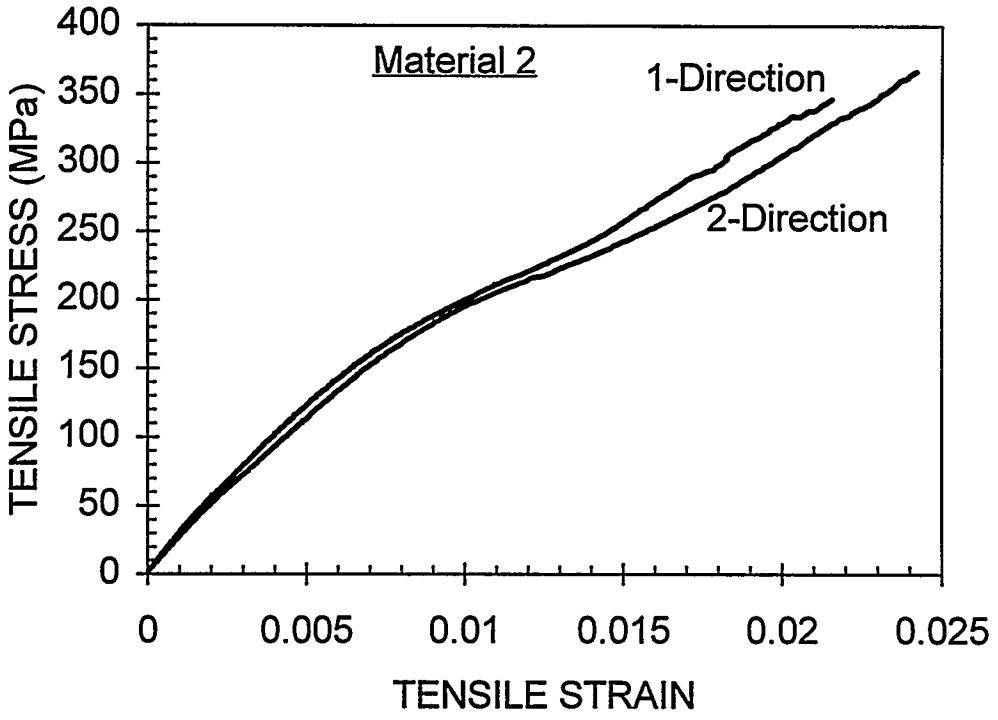

Fig. 8. Typical in-plane tensile stress-strain response of Material 2 for monotonic loading in the laminate principal directions.

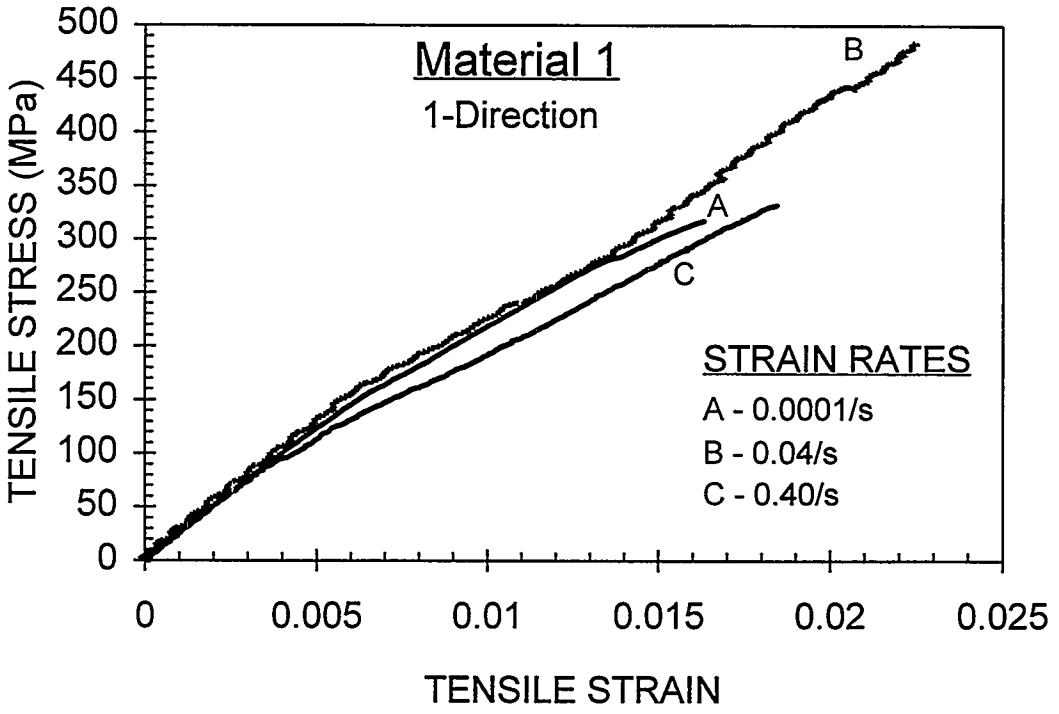

Fig. 9. Typical in-plane tensile stress-strain response of Material 1 in the 1-direction as a function of strain rate. Specimens are 3.2 mm thick.

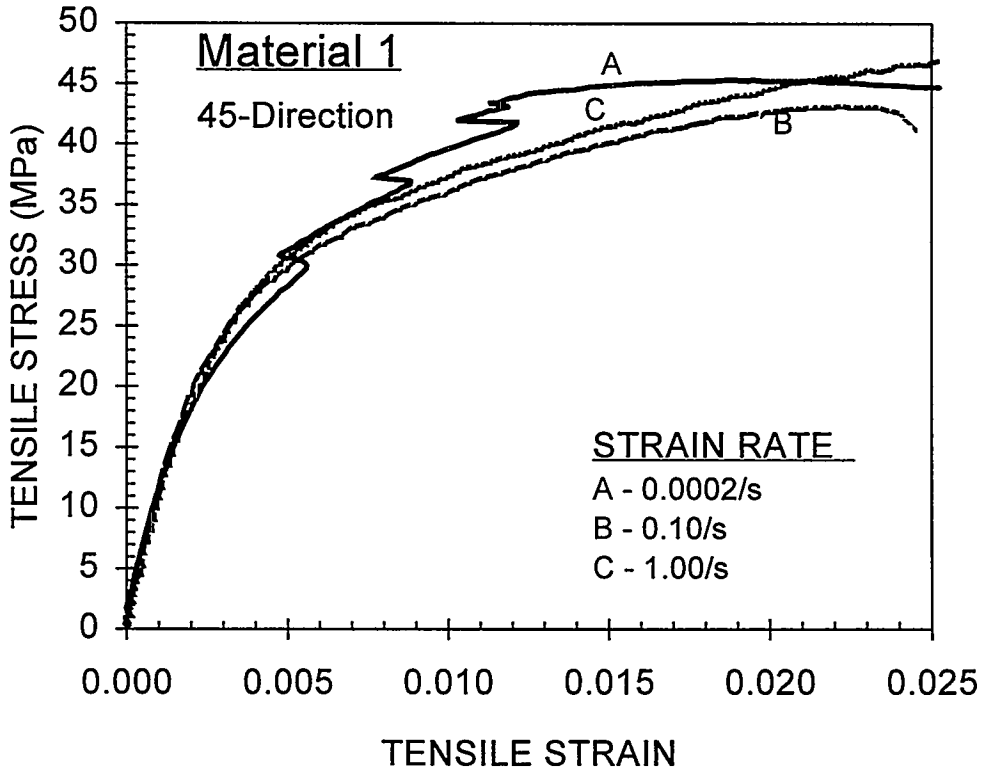

Fig. 10. Typical in-plane tensile stress-strain response of Material 1 in the 45° off-axis direction as a function of strain rate. Specimens are 3.2 mm thick.

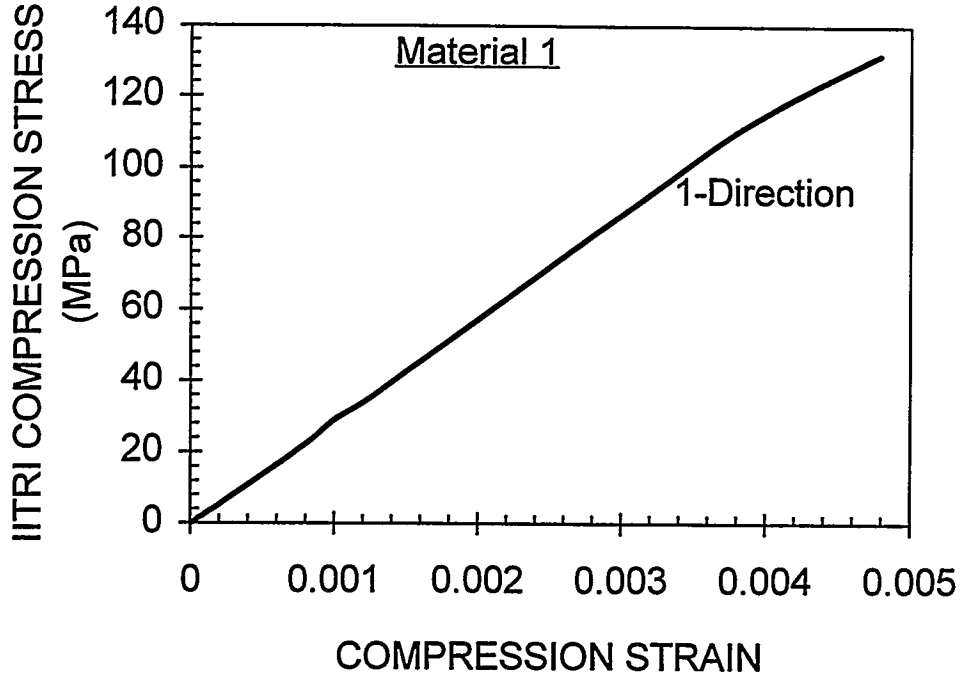

Fig. 11. Typical in-plane IITRI compression stress-strain response of Material 1 in the 1-direction.

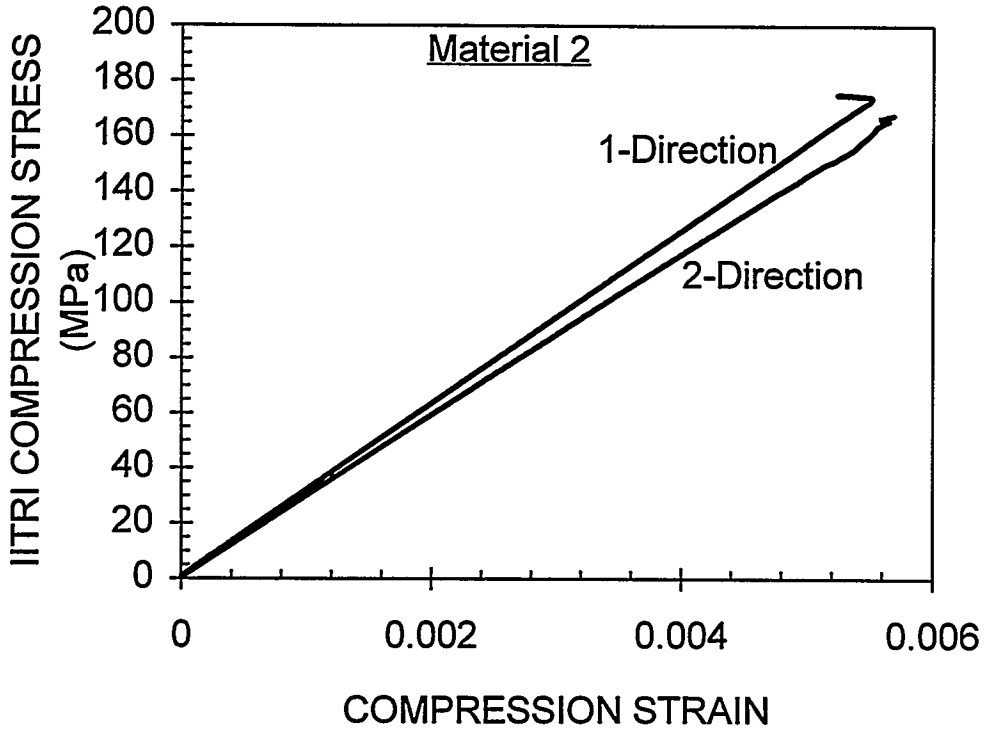

Fig. 12. Typical in-plane IITRI compression stress-strain response of Material 2 in the laminate principal directions.

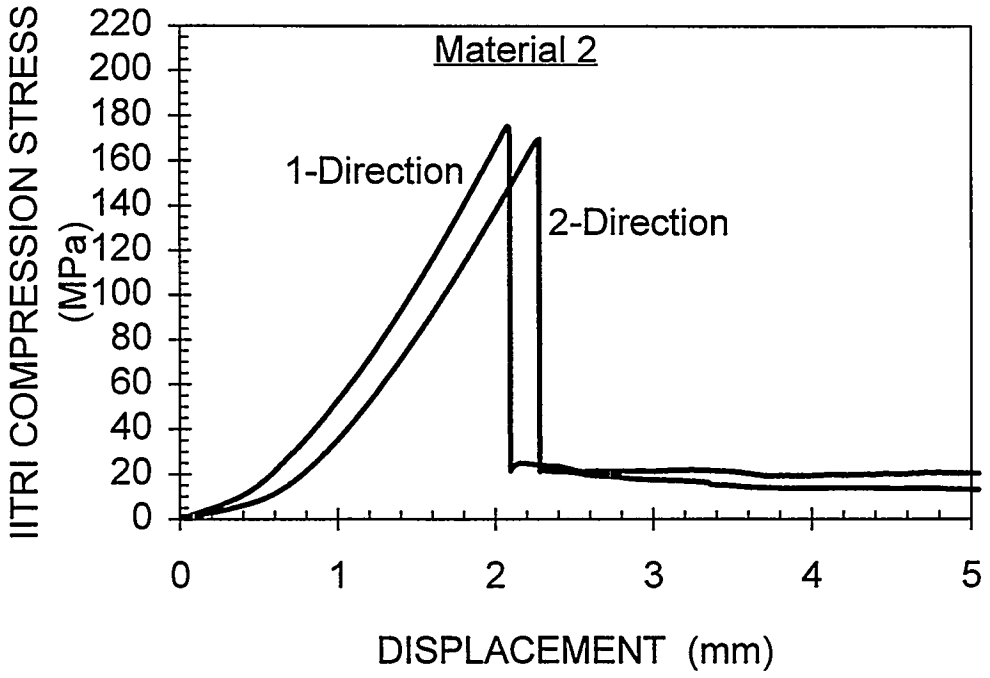

Fig. 13. Typical in-plane IITRI compression stress-crosshead displacement response of Material 2 in the laminate principal directions. Note that specimens carries approximately 20 MPa to large displacements following major load drop.

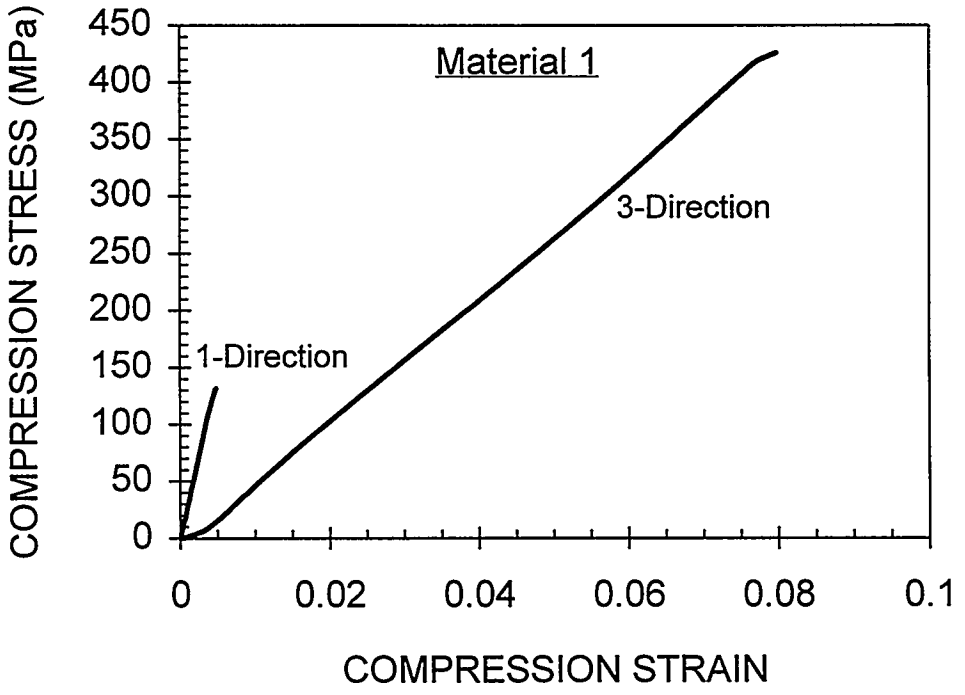

Fig. 14. Typical transverse compression stress-strain response of Material 1 in the laminate 3-direction (sometimes designated the transvere or through-the-thickness direction); 1-direction IITRI compression results shown for comparison.

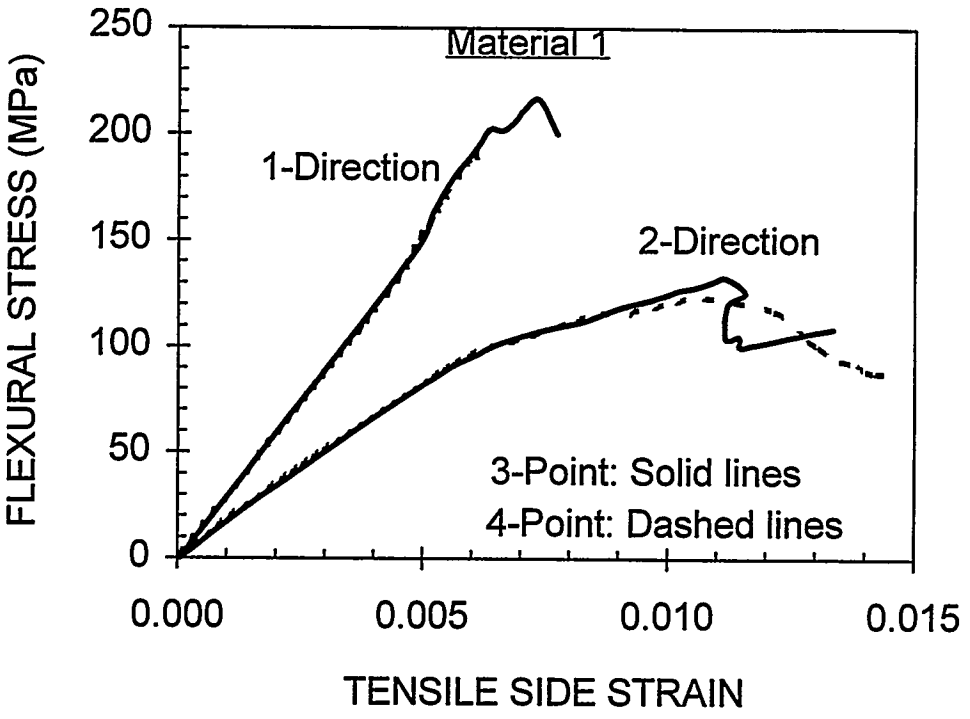

Fig. 15. Typical 3-point and 4-point flexural stress-strain response of Material 1 in the 1- and 2-directions of the laminate. Strains are measured on the specimen surface subjected to tensile stress.

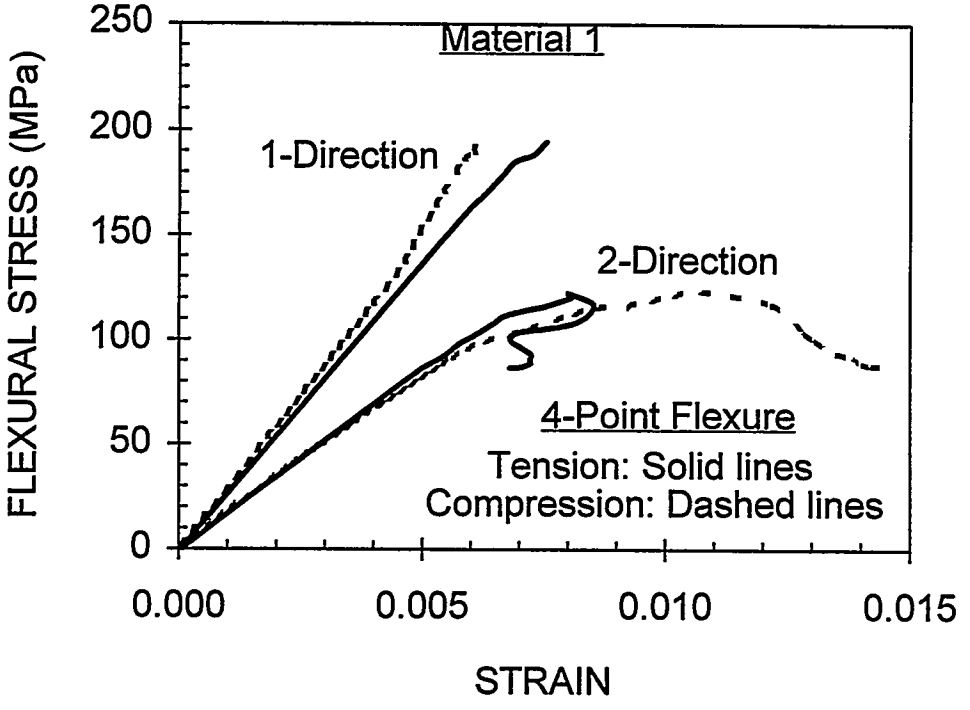

Fig. 16. Comparison of tension and compression surface responses of Material 1 specimens loaded in 4-point flexure. Data are shown for both 1- and 2-direction loadings.

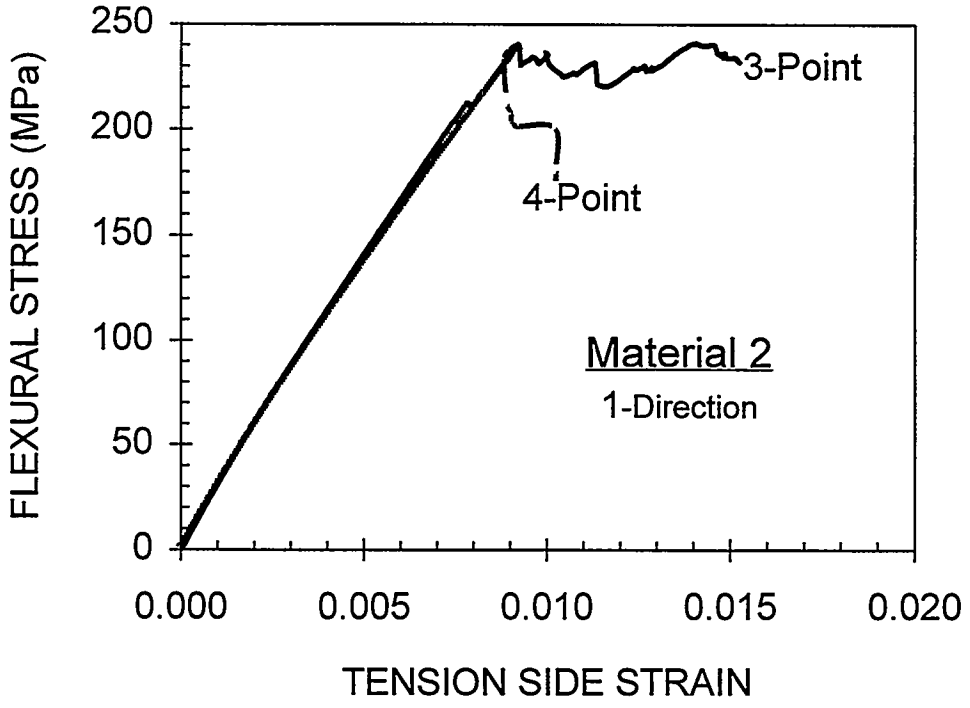

Fig. 17. Typical 3-point and 4-point flexural stress-strain response of Material 2 loaded in the 1-direction. Strains are measured on the specimen surface subjected to tensile stress.

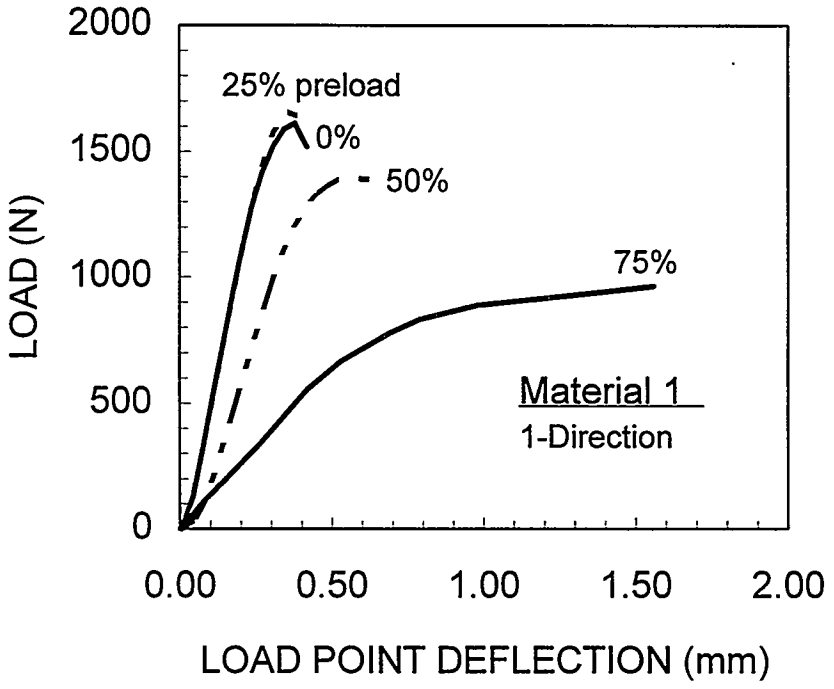

Fig. 18. Typical force vs. midspan deflection response as a function of tensile preload for Material 1 specimens subjected to short beam shear (SBS) loading. Preload level is relative to the 1-direction tensile stresses. Specimen span-to-depth ratio is about 5; the specimen depth is 6.3 mm.

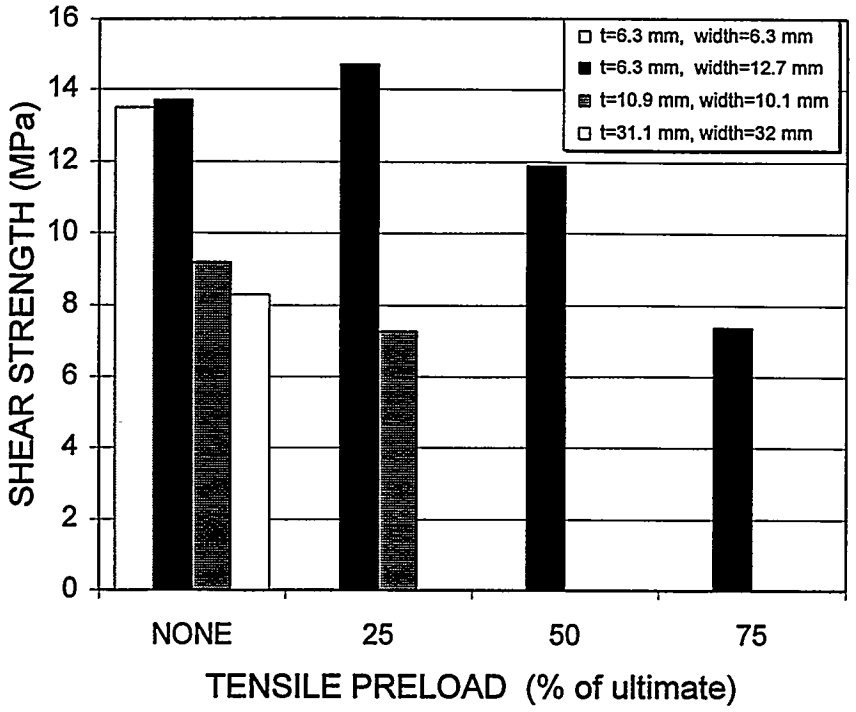

Fig. 19. SBS apparent shear strength as a function of tensile preload for Material 1 specimens with thicknesses of 6.3, 10.9 and 31.1 mm. Preload level is relative to the 1-direction tensile strength. Specimen span-to-depth ratio is about 5.

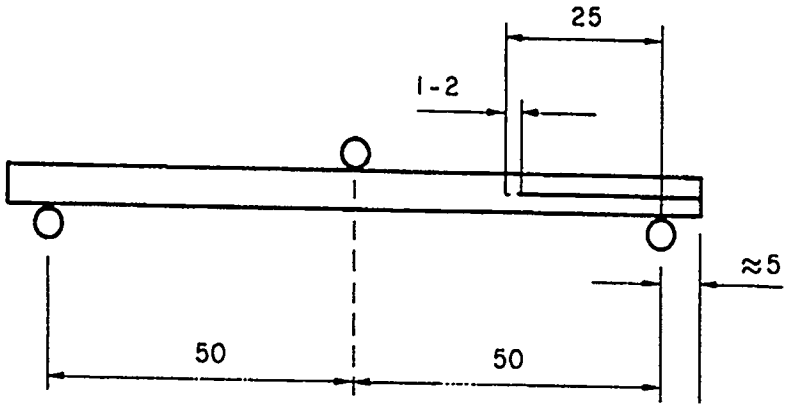

Fig. 20. Schematic of the end notched flexure (ENF) setup for Mode II (shear) fracture toughness tests. Dimensions in mm.

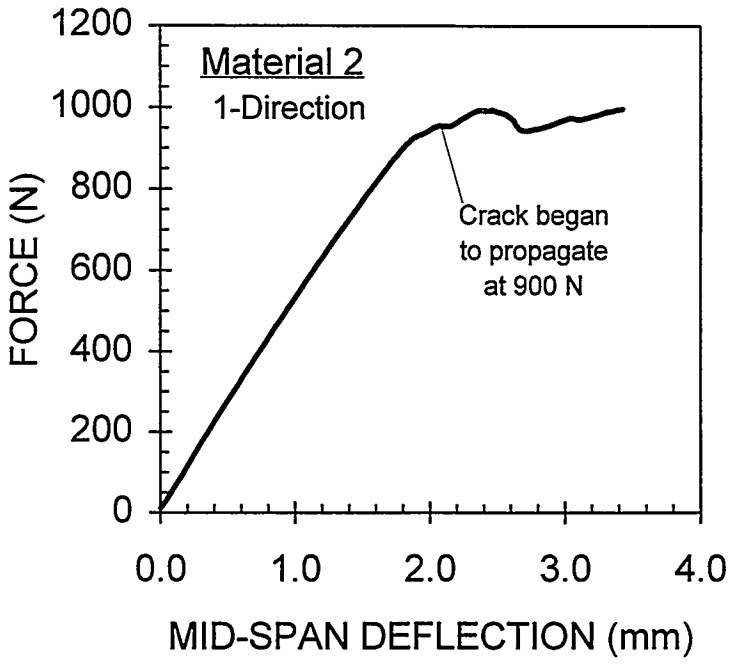

Fig. 21. Typical force vs. midspan deflection response of Material 2 ENF fracture toughness specimen loaded in 3-point flexure. Load at which crack propagation begins is used to calculate Mode II fracture energy for 1-direction specimen.

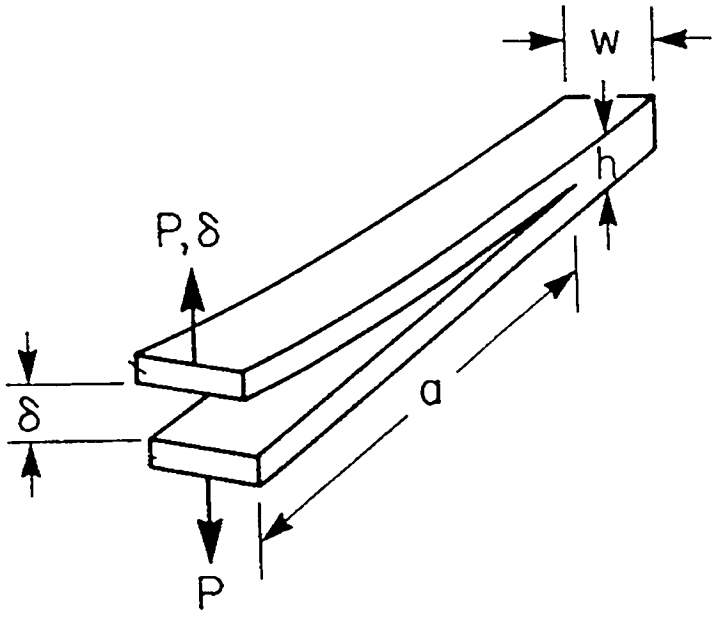

Fig. 22. Schematic of the double cantilever beam (DCB) setup for Mode I (opening) fracture toughness tests.

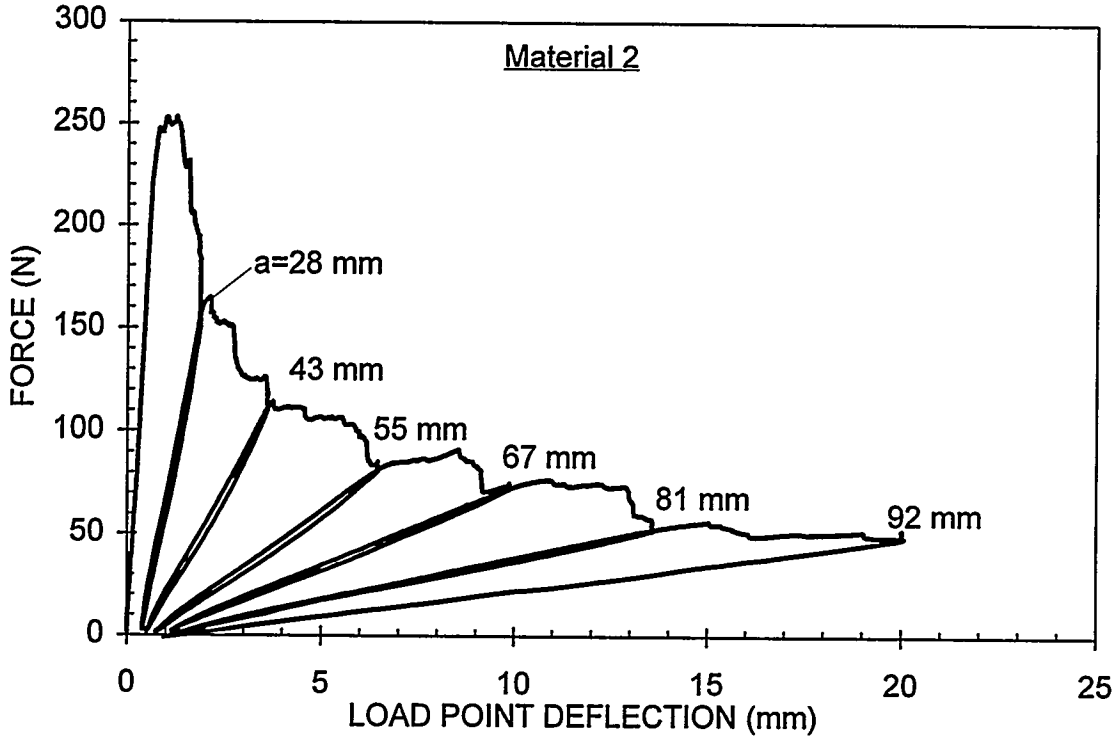

Fig. 23 Typical force vs. load point deflection response of Material 2 double cantilever beam (DCB) Mode I fracture toughness specimen subjected to multiple load/unload cycles. Crack length 'a' for each load cycle is indicated.

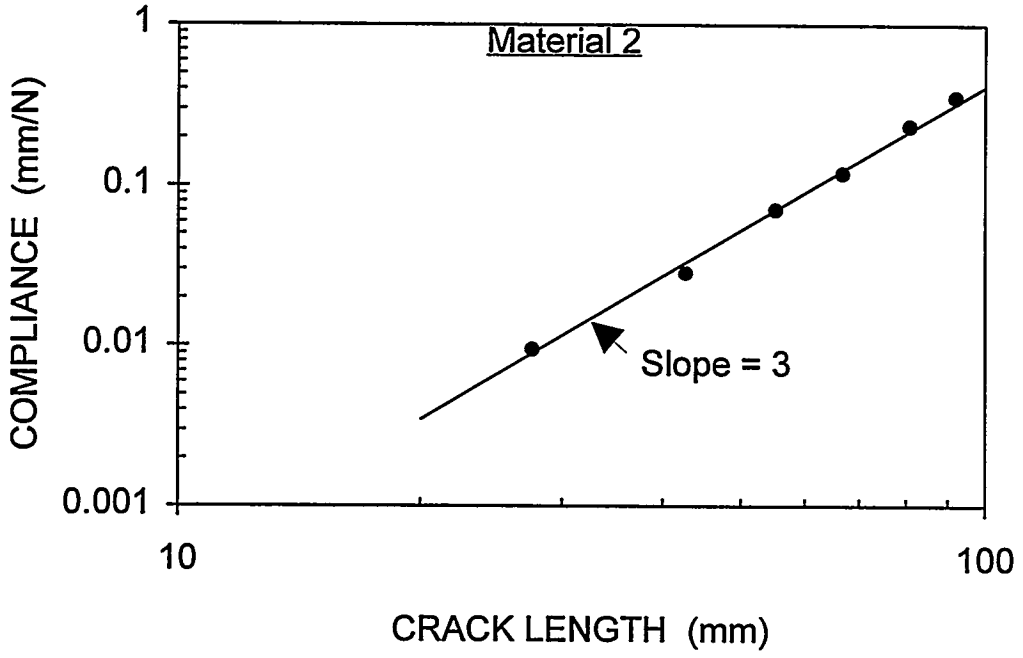

Fig. 24. Specimen compliance vs. crack length data from a single Material 2 DCB specimen tested for Mode I fracture toughness.

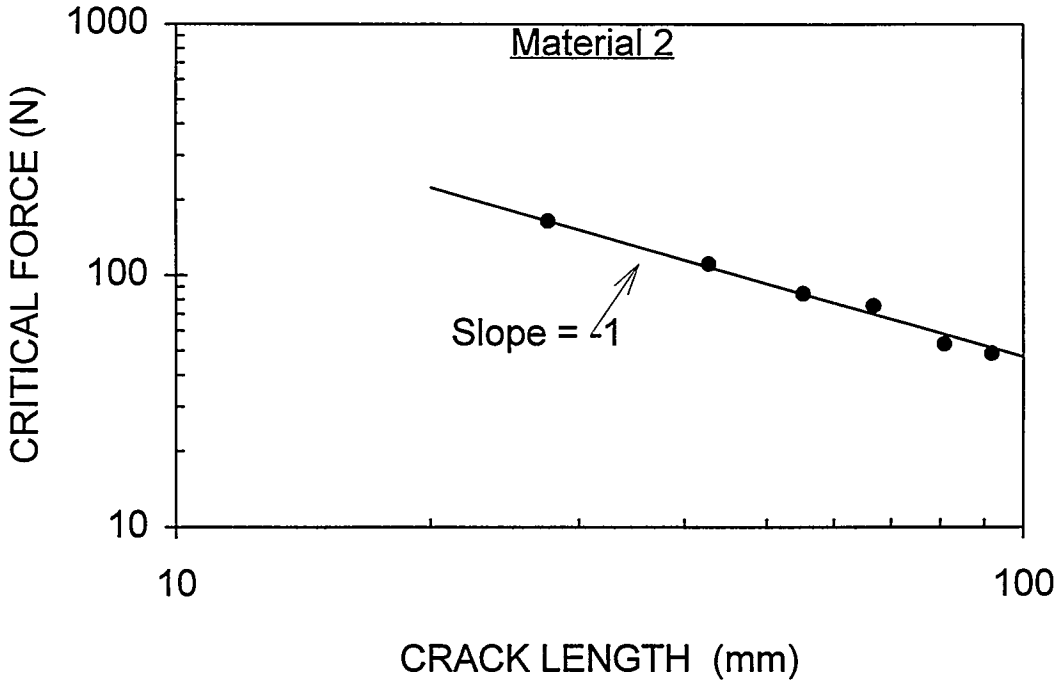

Fig. 25. Critical force vs. crack length data from a single Material 2 DCB specimen tested for Mode I fracture toughness.

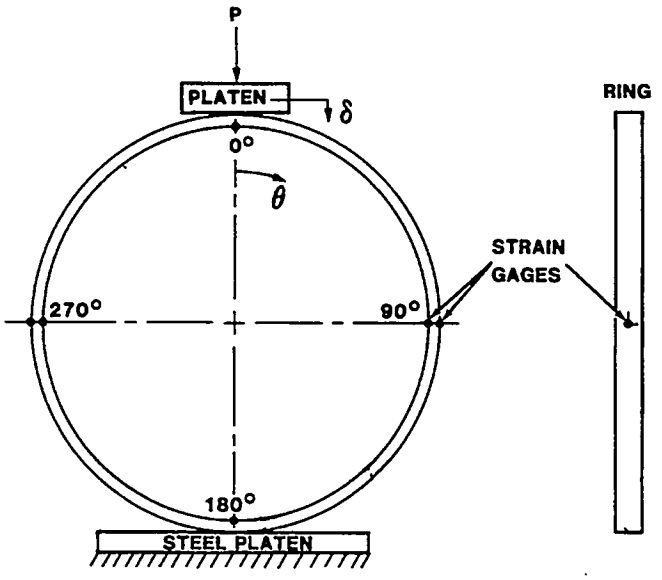

Fig. 26 Schematic of experimental setup for diametral compression of rings.

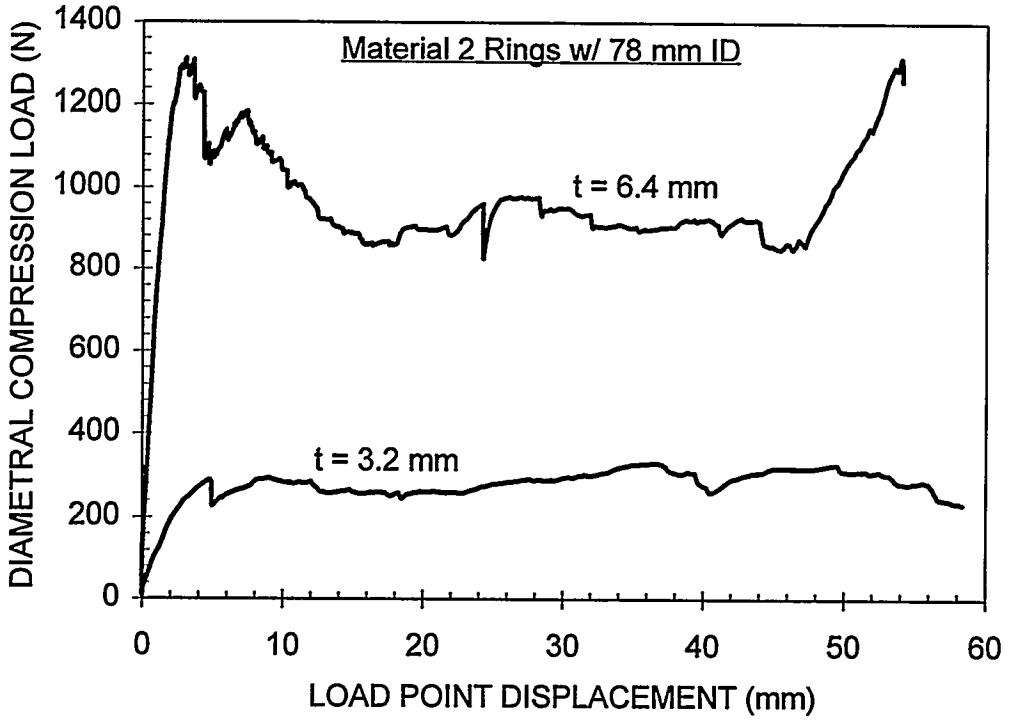

Fig. 27. Typical load vs. load point deflection response of Material 2 rings (78 mm inside diameter) subjected to diametral compression loading. Curves are shown for rings with wall thicknesses of 3.2 mm and 6.4 mm.

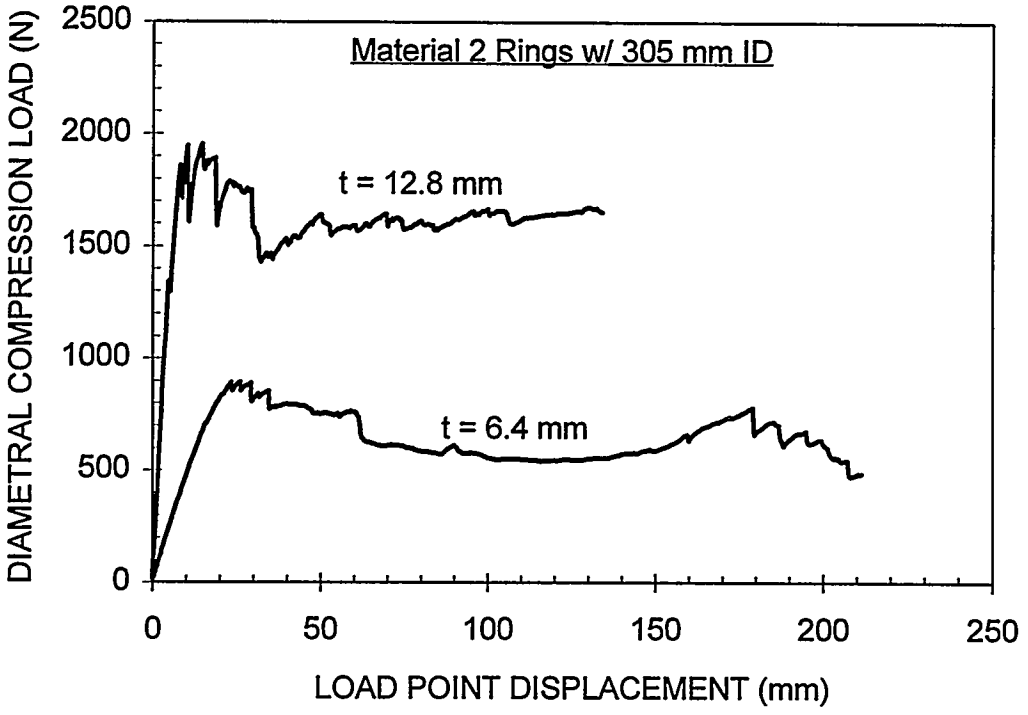

Fig. 28. Typical load vs. load point deflection response of Material 2 rings (305 mm inside diameter) subjected to diametral compression loading.

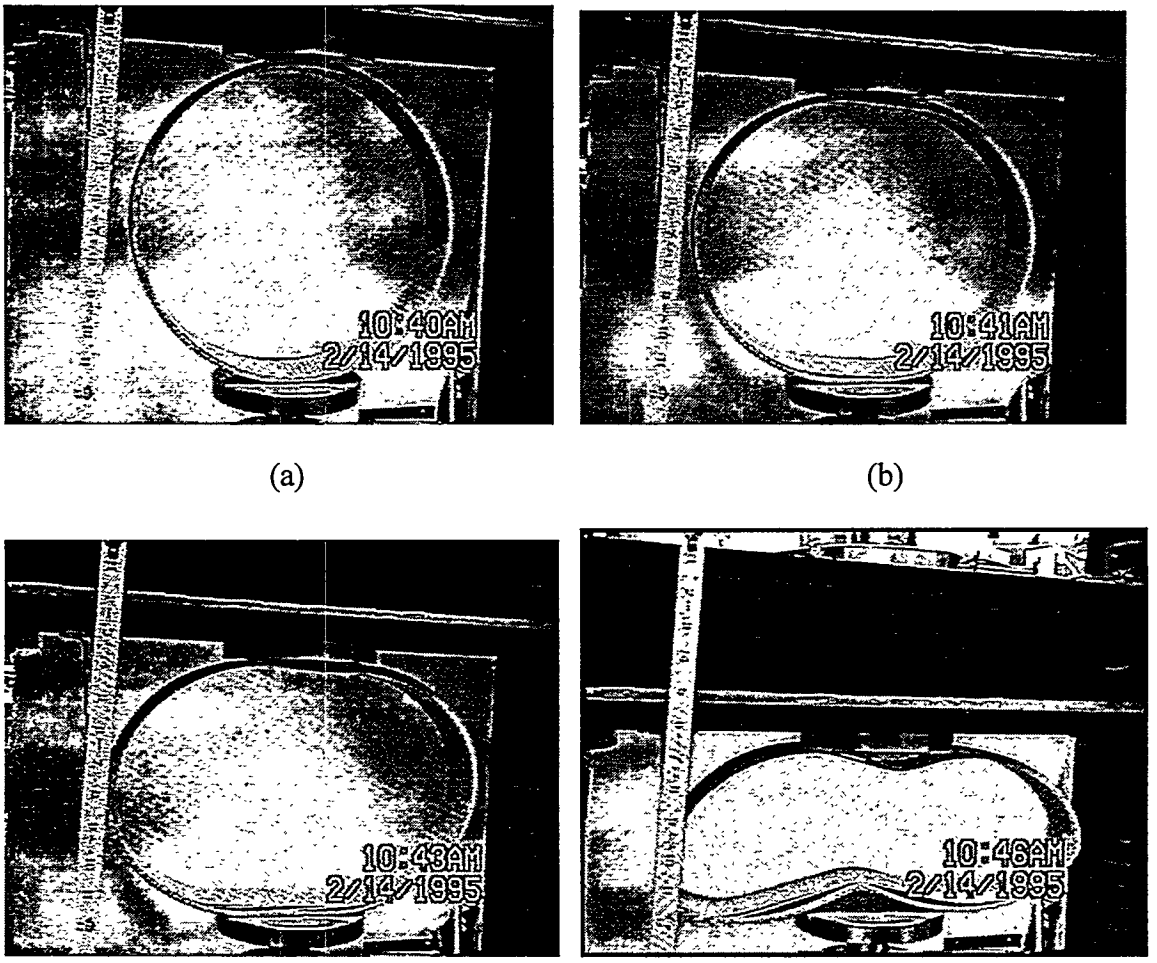

(a) (b)

(c) (c)

Fig. 29. Photograph showing a 305 mm ID ring of 6.4 mm thickness at different deflection levels during diametral compression test.

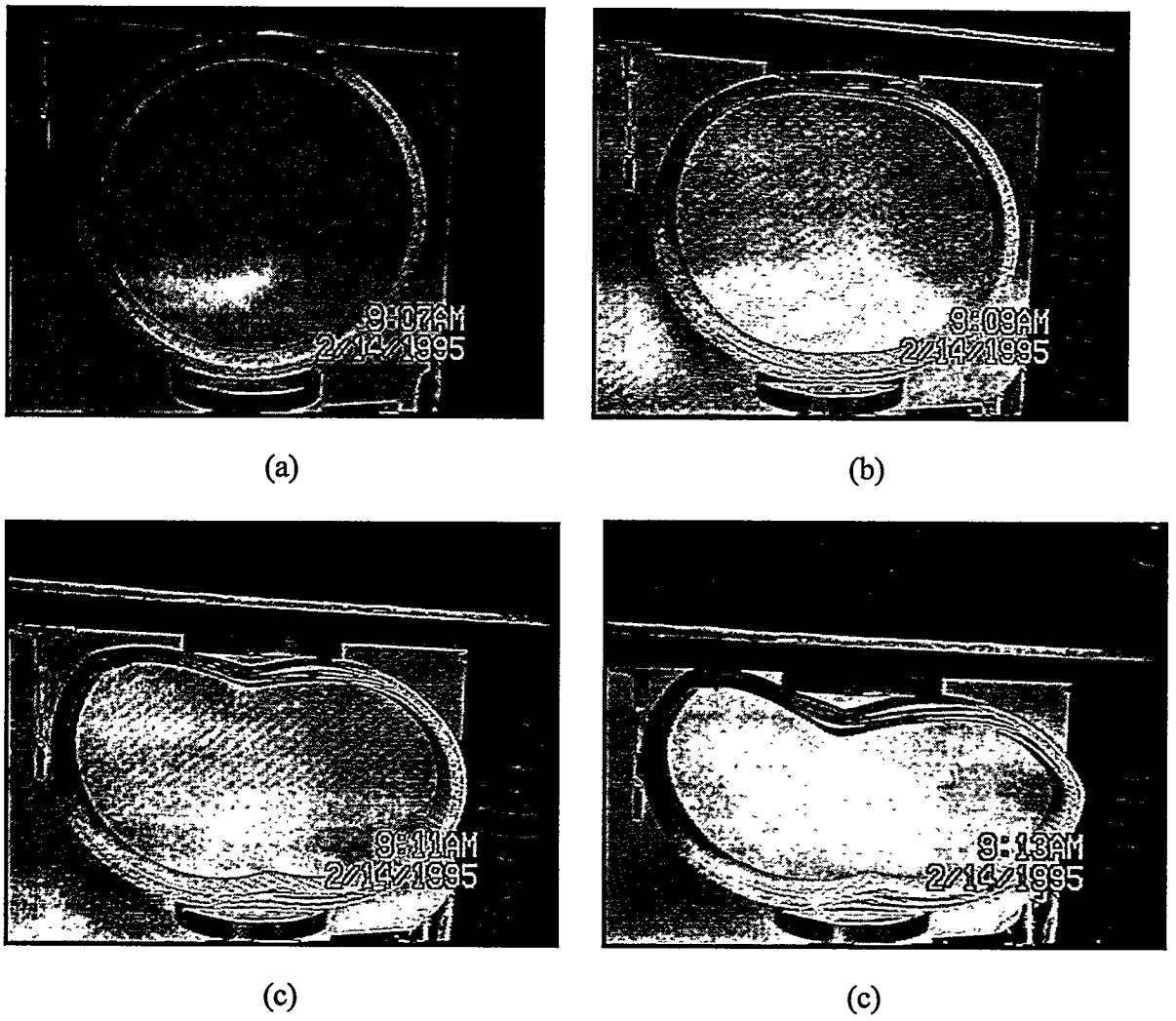

Fig. 30. Photograph showing a 305 mm ID ring of 12.8 mm thickness at different deflection levels during diametral compression test.

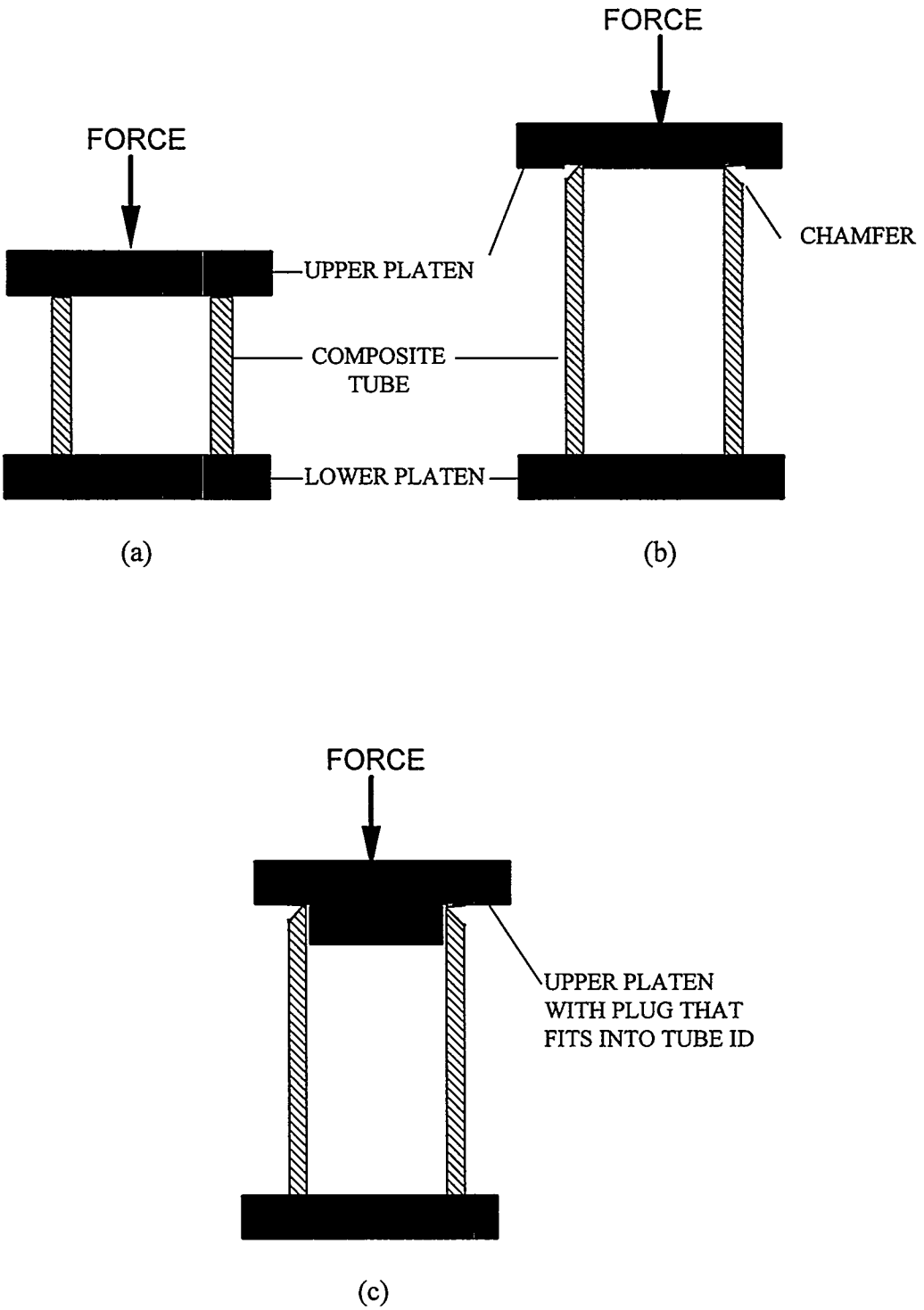

Fig. 31. Schematic of experimental setups for axial compression tests on Material 2 composite tubes: (a) tube ends without chamfer, (b) one end of tube with 45° chamfer and flat platens, and (c) tube with chamfer and upper platen with plug.

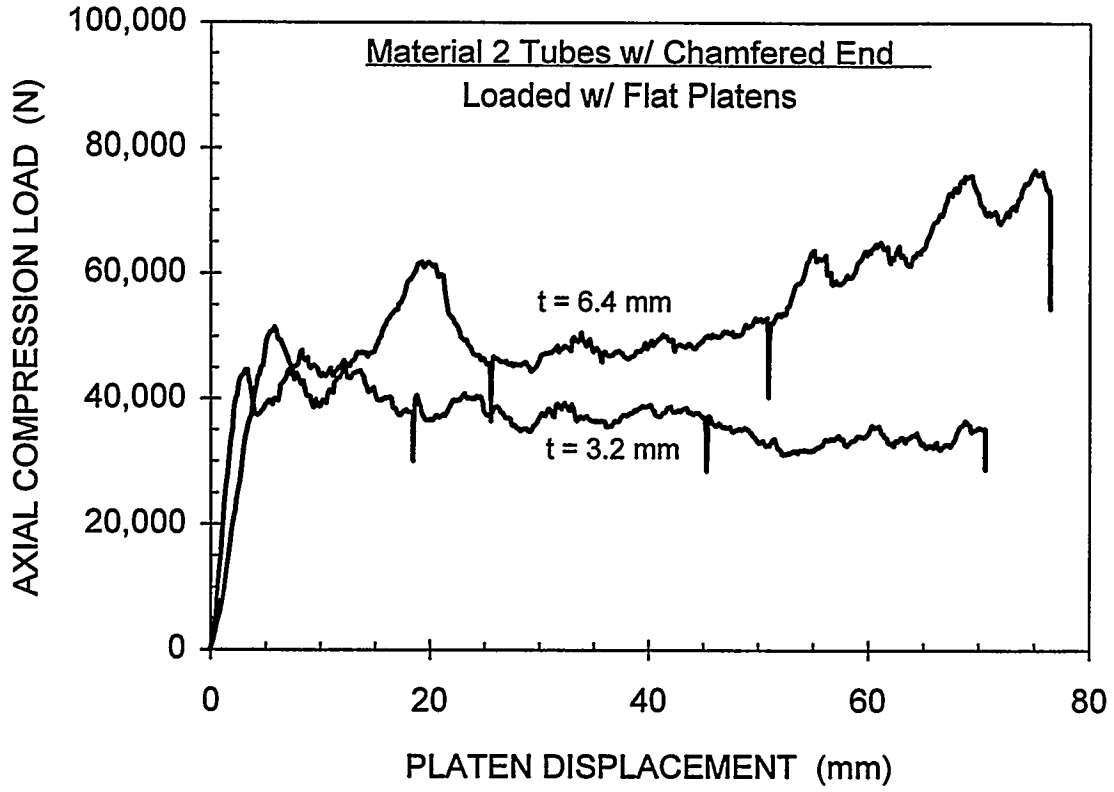

Fig. 32. Typical load vs. platen deflection response of Material 2 tubes (78 mm inside diameter and 142 mm length) subjected to axial compression loading. One end of the tube has a 45° chamfer; both ends are loaded with a flat platen. Curves are shown for tubes with wall thicknesses of 3.2 mm and 6.4 mm.

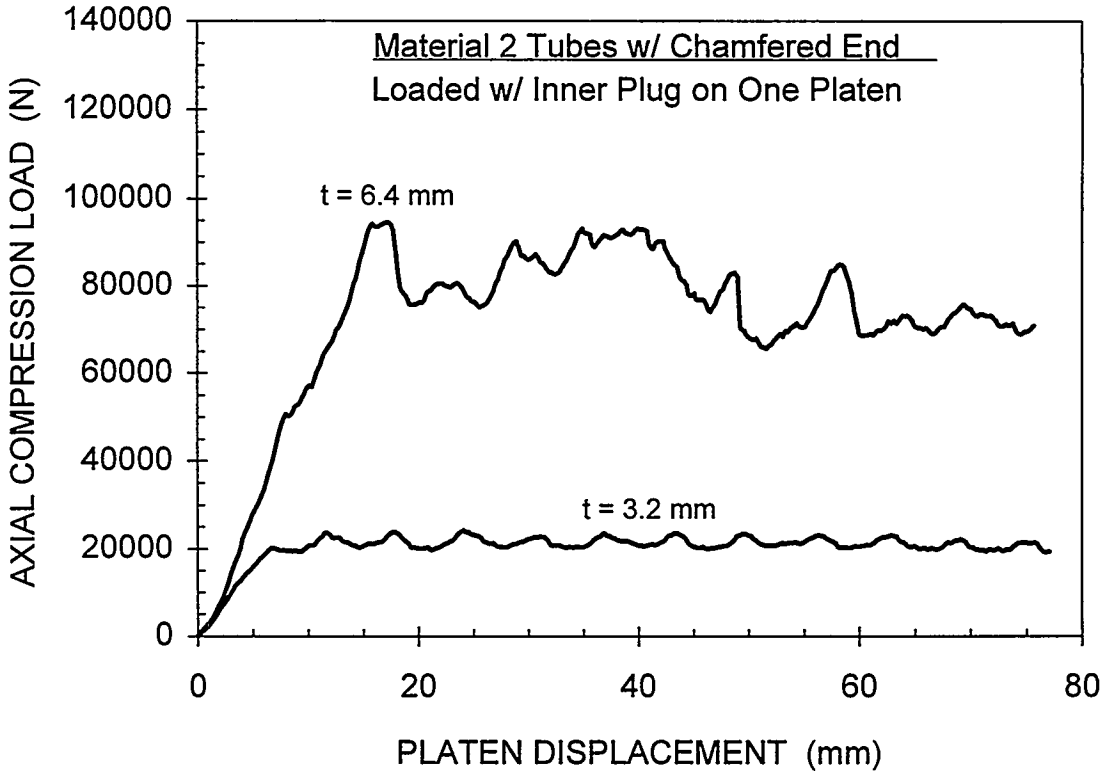

Fig. 33. Typical load vs. platen deflection response of Material 2 tubes (78 mm inside diameter and 142 mm length) subjected to axial compression loading. One end of the tube has a 45° chamfer. The platen loading the chamfered end has a short plug that fits into the tube ID; the other end of the tube is loaded with a flat platen. Curves are shown for tubes with wall thicknesses of 3.2 mm and 6.4 mm.

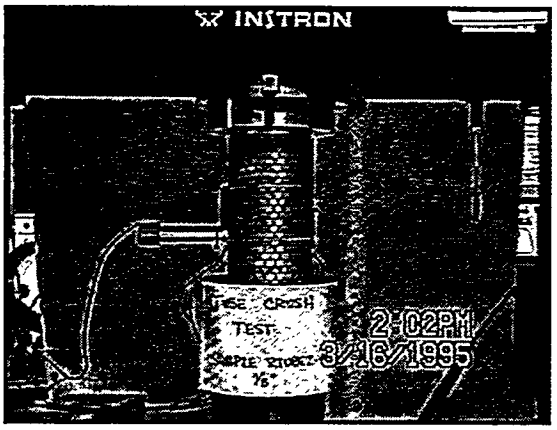

(a)

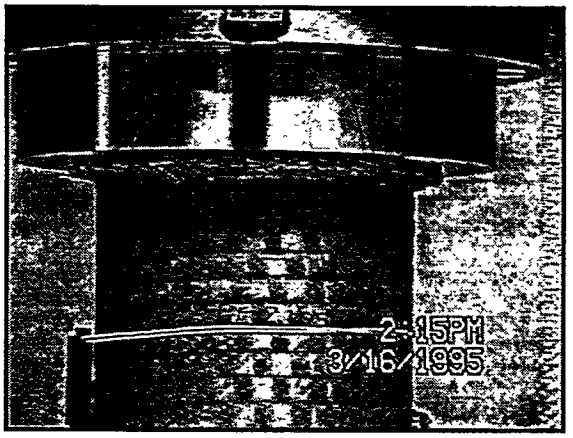

(b)

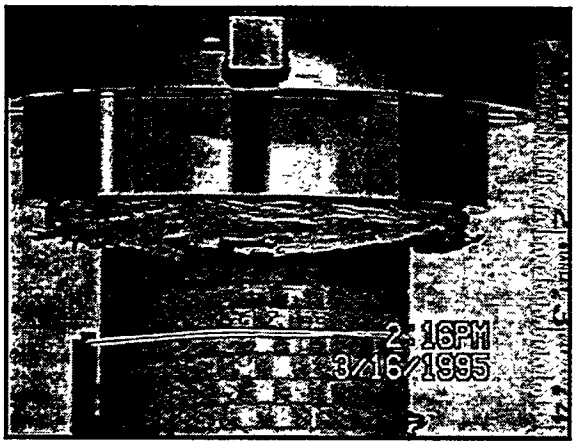

(c)

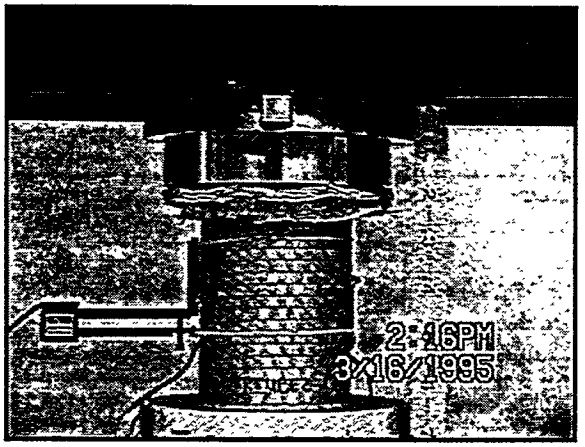

(c)

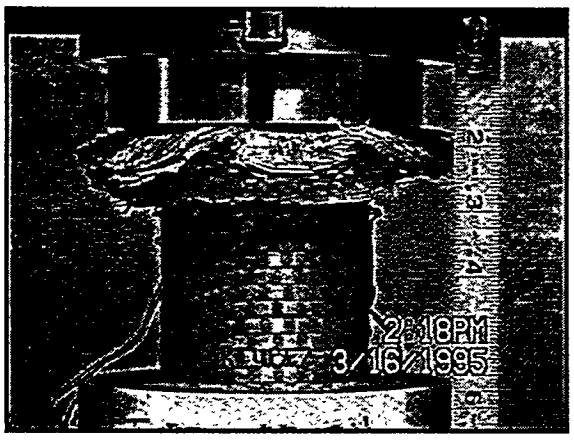

(d)

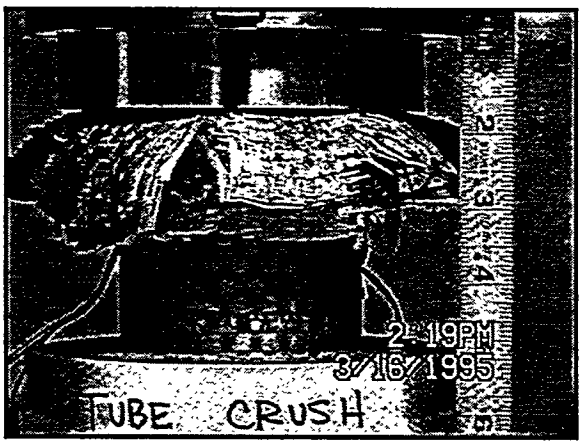

(e)

Fig. 34. Photograph showing Material 2 tube of 3.2 mm wall thickness at different deflection levels during diametral compression test. The top platen used to load this specimen (78 mm ID and 142 mm long) has a plug that fits into the tube ID.

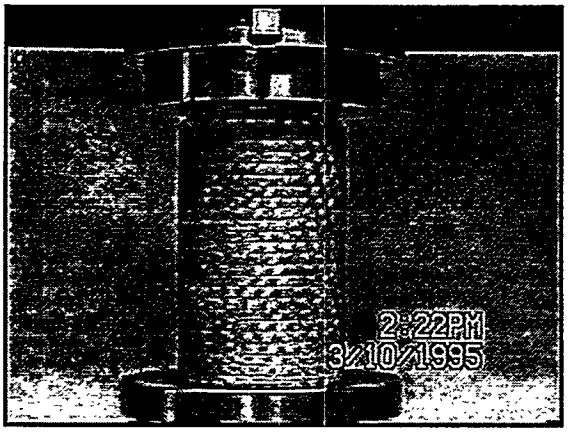

(a)

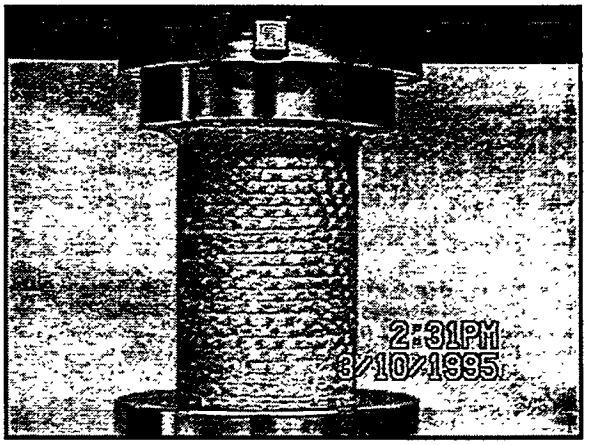

(b)

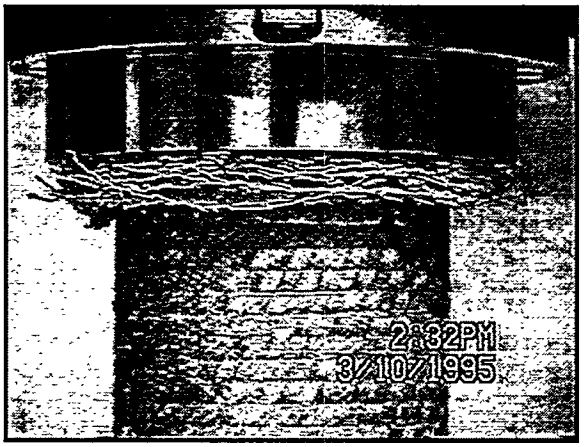

(c)

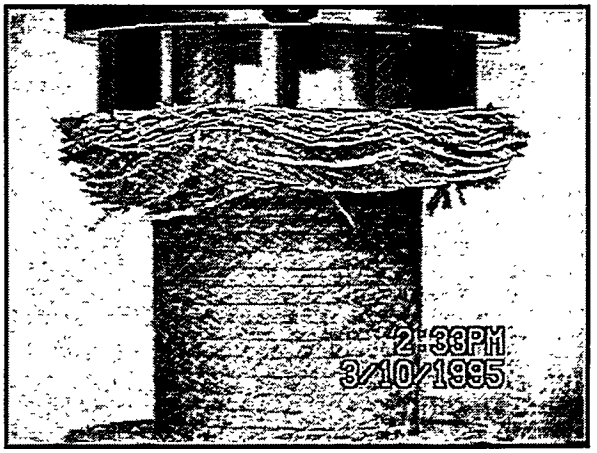

(c)

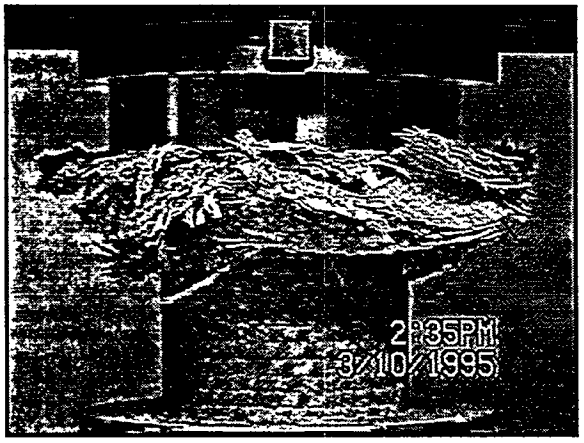

(d)

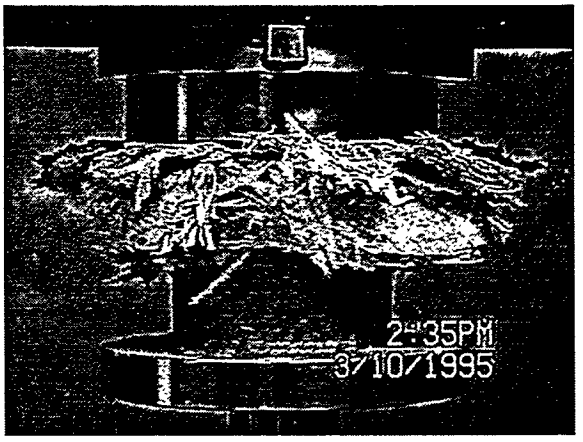

(e)

Fig. 35. Photograph showing Material 2 tube of 6.4 mm wall thickness at different deflection levels during diametral compression test. The top platen used to load this specimen (78 mm ID and 142 mm long) has a plug that fits into the tube ID.

DISTRIBUTION

UNLIMITED RELEASE:

MS 0320 LDRD Office, 4503
MS 0443 S. N. Burchett, 9117
MS 0437 J. B. Aidun, 9118
MS 0437 E. P. Chen, 9118
MS 0437 J. D. Gruda, 9118
MS 0437 D. Lo, 9118
MS 0437 F. J. Mello, 9118
MS 0437 K. E. Metzinger, 9118
MS 0437 E. D. Reedy, 9118 (20)
MS 0820 P. Yarrington
MS 0841 P. J. Hommert, 9100
MS 0960 J. Q. Searcy,1400
MS 0961 J. A. Sayre, 1403
MS 0958 J. L. Ledman, 1472
MS 0958 J. A. Brammer, 1472
MS 0958 E. A. Correa, 1472
MS 0958 M. W. Donnelly, 1472
MS 0958 J. A Emerson, 1472
MS 0958 T. R. Guess, 1472 (15)
MS 0958 M. E. Stavig, 1472 (5)
MS 9404 J. F. Wang, 8713
MS 9404 L. Domeier, 8230
MS 9402 J. Spingarn, 8230
MS 9042 P. E. Nielan, 8742
MS 9042 K. Trinh, 8742
MS 9044 W. A. Kawahara, 8746
MS 9018 Central Technical Files, 8523-2
MS 0899 Technical Library, 4414 (5)
MS 0619 Print Media, 12615
MS 0100 Document Processing For DOE/OSTI, 7613-2 (2)